The mafic-silicic layered intrusions of Saint-Jean-du-Doigt (France) and North-Guernsey (Channel Islands), Armorican Massif: Gabbro-diorite layering and mafic cumulate-pegmatoid association

Martial Caroff, Nolwenn Coint, Erwan Hallot, Cédric Hamelin, Jean-Jacque Peucat, Gilles Charreteur

The mafic-silicic layered intrusions of Saint-Jean-du-Doigt (France) and North-Guernsey (Channel Islands), Armorican Massif: gabbro-diorite layering and mafic cumulate-pegmatoid association

Martial Caroff [a,*], Nolwenn Coint [a,1], Erwan Hallot [b], Cédric Hamelin [a,2], Jean-Jacques Peucat [b], Gilles Charreteur [b]

[a] UMR CNRS 6538 « Domaines Océaniques », IUEM, Université de Brest, 6 avenue Victor Le Gorgeu, CS 93837, 29238 Brest cedex 3, France

[b] Géosciences Rennes, UMR CNRS 6118, Université de Rennes 1, 35042 Rennes cedex, France

* Corresponding author: caroff@univ-brest.fr

[1] Present address : Department of Geosciences, Texas Tech University, Lubbock, TX 79409, USA (nolwenn.coint@ttu.edu)

[2] Present address : IPGP, Laboratoire de Géosciences Marines, 4, Place Jussieu 75252 Paris cedex 05, France

Abstract

The Saint-Jean-du-Doigt (France) and North-Guernsey (Channel Islands) Intrusive Complexes (hereafter referred to as SJIC and NGIC, respectively) are examples of mafic-silicic layered intrusions in the Armorican Massif. Both are characterized by the occurrence of (1) a basal/peripheral gabbroic unit interlayered with sheets (generally dioritic in composition, occasionally gabbroic) and crossed by leucocratic diapirs and pipes (from monzodioritic to Q-monzonitic in composition), (2) peripheral pegmatoids associated with mafic cumulates and (3) coeval granitoids. Beside these main similarities, some contrasted features lead us to propose two distinct models of formation. The Variscan SJIC includes tholeiitic mafic rocks (monzogabbro) that locally mingle and mix with leucocratic components (monzonite or Q-monzonite). The Cadomian NGIC is calc-alkaline. The SJIC sheet-bearing gabbro is homogeneous from a petrologic point of view, whereas the NGIC exhibits gabbroic macrorhythmic sequences with mineral layering. The Sr-Nd isotopic compositions of the SJIC gabbros are significantly different from those of the associated dioritic layers. This is not the case in the NGIC where the magmas could be cogenetic. We argue that the SJIC gabbro was a liquid that crystallized *in situ* without significant crystal settling. By contrast, the rhythmic sequences of the NGIC are consistent with crystal accumulation. Subsequently, both can be seen as mafic reservoirs which were repeatedly invaded by magmas of intermediate composition. We interpret the sheets in the SJIC as the result of horizontal spreading of dioritic metastable magmas into a gabbroic reservoir crystallizing from below, at levels of neutral buoyancy. Injections and convection in the central part of the reservoir possibly resulted in spectacular mixing/mingling structures. In the NGIC, the emplacement of the dioritic sheets was rather controlled by pre-existing rhythmic cumulative structures. In both intrusions, late differentiated diapirs were extracted from the dioritic sheets. Associated

peripheral pegmatoids are thought to result from the crystallization of liquids issued from a mafic intercumulus melt in the presence of a fluid phase. This extraction might have been enhanced by the disruption of the peripheral cumulate stack, perhaps following pressure drops.

Keywords: Gabbro; Diorite; Granite; Layered intrusion; Replenishment; Armorican Massif

1. Introduction

The term MASLI (MAfic-Silicic Layered Intrusion), as first proposed by Wiebe (1993a and b), refers to plutonic complexes with interlayered mafic (gabbroic) and intermediate/felsic (dioritic to granitic) rocks (Wiebe, 1996; Franceschelli et al., 2005). MASLIs can be recognized by distinctive field relationships which always include (i) lobate contacts between the main gabbro-dioritic intrusions and surrounding or underlying granitic/granodioritic plutons and (ii) layers, sheets, diapirs, and/or veins of dioritic/silicic material into gabbroic units (Wiebe, 1996). Other features commonly (but not always) described in such complexes are: (iii) macrorhythmic gabbro-dioritic units, from less than one to several tens of meters thick, with chilled bases (Wiebe, 1993b, 1994, 1996; Waight et al., 2007), (iv) modal layering and feldspar lamination in the dioritic/silicic layers (Wiebe, 1996), (v) mafic/intermediate enclaves in the granites (Wiebe, 1994; Wiebe et al., 1997), and (vi) basaltic pillow-like chilled bodies within felsic units (Wiebe, 1974, 1993b; Wiebe et al., 2001). Although differences exist between the examples, Wiebe and others first proposed a comprehensive model to account for these features: repeated mafic injections into a felsic chamber, from dioritic to granitic composition, followed by fractional crystallization and complex liquid-liquid (and/or partially crystallized magma-magma) interactions including

70 small scale diapirism and hybridization. More recently, MASLIs were recognized to result
71 from multiple replenishments of mafic and felsic magmas, mingling and limited mixing, and
72 rejuvenation of granite (Wiebe et al., 2007).

73 If the Cadomian layered gabbro-diorite complex of North-Guernsey (Channel Islands)
74 was suspected by Wiebe (1996) to be a MASLI, the Variscan intrusion of Saint-Jean-du-Doigt
75 (France) was never considered as such. However, both Armorican plutonic bodies display
76 many of the features characteristic of mafic-silicic layered intrusions. Additionally, both
77 complexes show spectacular pegmatoid (gabbroic pegmatite) occurrences systematically
78 associated with coarse-grained mafic cumulates. Such a lithologic association has already
79 been described in various gabbroic intrusions (Smartville intrusive complex, California:
80 Beard and Day, 1986; Kraemer macrodyke, Greenland: Momme and Wilson, 2002; Mount
81 Sheridan gabbro, Oklahoma: McEllen, 2006), but not specifically in MASLIs. In spite of their
82 similarities, each Armorican intrusion shows distinctive petrological and geochemical
83 (isotopic) characters.

84 The aim of this study is to reexamine the published models of MASLI formation
85 through these two new examples from the Armorican Massif, which display both shared and
86 contrasted features. This leads us to propose distinct processes of construction emphasizing
87 the possibility that replenishment of mafic chambers by intermediate partially crystallized
88 magmas explains some features of MASLIs.

89

90 **2. Analytical techniques**

91

92 Compositions of mineral phases were obtained with a Cameca SX50 automated
93 electron microprobe (Microsonde Ouest, Brest). Analytical conditions were 15 kV, 15 nA,

94 counting time 6 s, correction by the ZAF method. Concentrations <0.3% are considered
95 qualitative.
96 Major and trace element compositions (Table 1) were measured at the University of
97 Brest on whole rock powders by inductively coupled plasma atomic emission spectrometry
98 (ICP-AES). Analytical methods are described in Cotten et al. (1995). Relative standard
99 deviations are <2% for major elements and <5% for trace elements. For the coarsest-grained
100 samples, a large quantity of rock was crushed in a steel jaw-crusher (e.g., 20 kg for the
101 pegmatoid SJ16). After the crushed rock was quartered, a representative split was pulverized
102 in an agate mill.
103 The Sr-Nd isotopic compositions were obtained from whole rock powders with a
104 Cameca TSN 206 mass spectrometer (Guernsey) and with a Finnigan MAT 262 mass
105 spectrometer (Saint-Jean-du Doigt) at Géosciences Rennes. Sr, Rb, Sm and Nd contents were
106 measured by isotope dilution except for the SJIC samples in which Rb was determined by
107 ICP-AES. Errors on $^{87}Rb/^{86}Sr$ and $^{147}Sm/^{144}Nd$ ratios are 2% and 1%, respectively. Details of
108 analytical procedures are described in Peucat et al. (1999). $^{87}Sr/^{86}Sr$ ratios were normalized to
109 the NBS 987 standard ($^{87}Sr/^{86}Sr = 0.71025$) and $^{143}Nd/^{144}Nd$ ratios to the AMES standard
110 ($^{143}Nd/^{144}Nd = 0.511963$). ε_{Nd} values, in Table 2, were calculated using $^{143}Nd/^{144}Nd_{CHUR} =$
111 0.51264 and $^{147}Sm/^{144}Nd_{CHUR} = 0.1967$. They correspond to: $\varepsilon_{(0)} = 10^4((^{143}Nd/^{144}Nd_{sample}/$
112 051264) -1) and $\varepsilon_{(t)} = \varepsilon_{(0)} -(25.1((^{147}Sm/^{144}Nd_{sample} -1) /0.1967)\Delta_{(t)})$, following De Paolo
113 (1988).
114
115 **3. Saint-Jean-du-Doigt Intrusive Complex (SJIC)**
116
117 *3.1. Geology*

118

119 The Saint-Jean-du-Doigt Intrusion (SJIC) is located between the Trégor Cadomian
120 domain, mainly composed of volcanoclastic formations overlying a Palaeoproterozoic
121 (Icartian) gneissic basement (*c.* 2.0 Ga, Auvray et al., 1980), and the Léon Hercynian
122 metamorphic domain (Fig. 1a). The SJIC is composite and includes four main units: the
123 Primel cumulate-pegmatoid association, the Saint-Jean-du-Doigt monzogabbro-(Q-
124)monzonite mingled/mixed rocks, the Poul Rodou layered gabbro-diorites and several granitic
125 bodies (Fig. 1b). Some doleritic dykes cross cut the units, but were not found in the granitic
126 rocks. Most rocks have isotropic textures and exhibit no significant regional deformation
127 subsequent to their emplacement, with the exception of local brittle faulting. However, they
128 have undergone late- to post-magmatic alterations, resulting in the transformation of some
129 primary minerals, without significant change in bulk rock chemistry (Coint et al., 2008). The
130 SJIC was emplaced under a lithostatic pressure of about 0.5 GPa, i.e. at *c.* 15 km depth
131 (amphibole geobarometry: Johnson and Rutherford, 1989 and Schmidt, 1992 *in* Coint et al.,
132 2008), within Proterozoic rocks and Devonian-Carboniferous sediments. Chantraine et al.
133 (1986) have reported a carboniferous U-Pb zircon age of *c.* 350 Ma for the gabbros (Deutsch,
134 unpublished) confirmed by Barboni et al. (2008, 2010), who obtained U-Pb zircon ages at 347
135 ± 4 Ma for the mafic units and the granitic bodies from Poul Rodou. The SJIC was later
136 intruded by red granites at *c.* 300 Ma (Fig. 1b). The SJIC mafic rocks have a tholeiitic affinity
137 (Chantraine et al., 1986; Coint et al., 2008, 2009; see also section 5.2). Geochemical features
138 of intermediate/felsic rocks are rather typical of calc-alkaline suites (Barboni et al., 2010;
139 Capdevila, 2010).

140

141 *3.2. Coastal SJIC from East to West*

142

143 The Saint-Jean-du-Doigt Intrusive Complex is best exposed along the northern
144 shoreline. Field observations have been made from Poul Rodou to Primel through the bay of
145 Saint-Jean-du-Doigt (Fig. 1b).
146
147 *3.2.1. Poul Rodou: gabbro-diorite layering*
148 From southeast to northwest, the Poul Rodou cross-section begins with a small
149 granitic body in sharp intrusive contact with a Proterozoic formation (Fig. 1b and 2a). The
150 granite is equigranular and intrudes an intergranular/oikocrystic gabbro. Lobate contacts
151 between the granite and the adjacent gabbro and gabbroic enclaves within the granite are
152 interpreted as evidence for the contemporaneous crystallization of both magmas. Other
153 granitic intrusions crop out along the shoreline, such as the Beg ar Fri granite (sample SJ22,
154 Fig 1b and 2a). Several sub-parallel leucocratic sheets form layers within the gabbro. They are
155 oriented SE-NW and dip slightly (10° to 30°) toward the northeast. They are cut
156 southeastward by the granitic intrusion (Fig. 2a). This demonstrates the lack of apparent direct
157 link between leucocratic sheets and granitic bodies. Leucocratic sheets are thin (a few
158 decimeters thick) and sparse near the edge of the complex. They become thicker (up to
159 several decimeters) and more abundant to the northwest. The spacing from one sheet to
160 another varies from several decameters to a few meters. The upper contact with the overlying
161 gabbro is systematically undulated, sometimes connected to felsic masses, a few decimeters in
162 size, within the overlying gabbro (Fig. 3a, b). When elongated, these structures are orientated
163 sub-perpendicularly to the sheet layers. They are interpreted as gravity-driven felsic diapirs
164 extracted from the sheets. In the present orientation, these instabilities are not sub-vertical and
165 the sheets are not sub-horizontal. The variable dipping angles of the structures along the Poul
166 Rodou shoreline are consistent with post-emplacement brittle deformation and denotes
167 northeastward tilting of blocks limited by NE-SW faults (Fig. 2a). The composition of the

168 leucocratic sheets is dioritic, with the exception of their upper part, sometimes Q-monzonitic
169 (Table 1). All are moderately cumulative in plagioclase (cumulus from 20% at the base to
170 50% at the top of the sheets) and generally exhibit an intergranular texture. Felspar-rich
171 (plagioclase and orthoclase) diapirs, more differentiated than their related sheets, have
172 textures ranging from intergranular to pegmatitic. Contrasting with the upper contacts, bases
173 of the leucocratic sheets form relatively regular surfaces with the underlying gabbro. Some
174 sheets are connected from below to sub-perpendicular pipe-like feeding structures (Fig. 3b
175 and c). In addition, when diapirs came near an overlying sheet, they could merge with it.
176 Alternatively, some diapirs did not intersect the overlying sheet but formed concave-down
177 structures (Fig. 3d). Except near Beg ar Fri, where an amphibole-rich cumulate has been
178 sampled (SJ44b, Fig. 2a), the gabbro is structurally and texturally homogeneous throughout
179 the Poul Rodou shoreline: no chilled margins, macrorhythmic units, or upward petrographic
180 gradation were observed.
181
182 *3.2.2. Saint-Jean's bay: monzogabbro-monzonite interactions*
183 The coast north of Saint-Jean-du-Doigt exposes spectacular and various monzogabbro-
184 (Q-)monzonite (see section 3.3 for rock nomenclature) interaction structures resulting from
185 brittle brecciation to mixing (producing hybrid rocks) through mingling (during which the
186 magmatic end-members retain their identity). At Saint-Jean's bay, angular breccias are
187 present only east of the dextral fault *F* (Fig. 1b) whereas mingling/mixing predominates
188 westward. Lobate structures are also visible in the transition zone to the Poul Rodou layered
189 gabbro-diorite unit.
190 Structures that result from ductile interactions between coexisting magmas include
191 pillowed mafic enclaves with chilled margins enclosed in a heterogeneous monzogabbro
192 (mingling, Fig. 4a), hybrid magmas (pure mixing), and banded rocks in the process of

193 hybridization (mingling/mixing, Fig. 4b). In partly hybridized rocks, several mafic enclaves
194 show diffuse margins. These interactions can be observed from microscopic (less than one
195 millimeter) to outcrop scales (several tens of meters). Locally, mafic enclaves present a
196 N40°E preferred orientation, suggesting ductile deformation in protoshear zones.
197 The angular facies consist of jigsaw-type breccias where polyhedral mafic enclaves are
198 enclosed in intermediate rocks forming a vein network (Fig. 4c). The veins are texturally
199 homogeneous intergranular (Q-)monzonites whereas a few blocky clasts exhibit
200 mixing/mingling features.
201
202 *3.2.3. Primel: cumulate-pegmatoid association*
203 Pegmatoids (gabbroic pegmatites), generally associated with plagioclase-phyric
204 cumulates, are distributed from Roc'h Louet to Primel (Fig. 1b). Cumulates are well exposed
205 at Roc'h Louet (Fig. 2b), whereas the coarsest-grained pegmatoid, containing large amphibole
206 crystals (up to 15 centimeters in length) and smaller plagioclase crystals, occurs westward
207 near the Primel red granite (Fig. 2c). There, pegmatoids occur as pods or veins within mafic
208 heteradcumulates with variable plagioclase contents. They are sometimes zoned, with an
209 amphibole-richer core. Pegmatoids are often more altered than the host gabbro. The cumulate-
210 pegmatoid association is bordered southward and southeastward by the monzogabbro-(Q-
211)monzonite unit of Saint-Jean. In this area, monzogabbros are locally rich in feldspar
212 megacrysts, similar to those described by Wiebe and Collins (1998) and Collins et al. (2006)
213 in the Devonian Kameruka Granodiorite (Bega batholith, southeastern Australia). Fine-
214 grained pegmatoids are found as patches or thin veins in mingled monzogabbro-(Q-
215)monzonite at Saint-Jean's bay western edge (Fig. 2b). In this zone, mottled pegmatoids have
216 also been observed. They are characterized by recrystallized amphibole-bearing flecks from 2
217 to 5 cm in diameter (see section 3.3).

Gabbroic aplites are often intimately associated with pegmatoids as patches or irregular veinlets (Fig. 4d). They are distinct from the doleritic dykes, which display sharp intrusive contacts with host rocks and have chilled margins.

In sample PM2 (Fig. 4d), an aplitic vein separates the pegmatoid from the cumulate, the latter being edged by a dark reaction zone.

3.3. Petrology

According to the recommendations of the IUGS, the nomenclature of plutonic rocks is based on modal compositions. As not all the primary phases are preserved, we have chosen to use the R1-R2 chemical discrimination diagrams of La Roche et al. (1980), as utilized by many authors (e.g., López-Moro and López-Plaza, 2004; Hellström et al., 2004).

At Poul Rodou, the SJIC rocks plot within the following fields of a R1-R2 diagram: olivine gabbro; diorite, monzodiorite and (Q-)monzonite (sheets and diapirs); and granite (intrusions). The Saint-Jean's bay samples plot as follow: olivine gabbro (doleritic dykes); monzogabbro, monzonite, and Q-monzonite (mixing/mingling facies). At Primel, pegmatoids are olivine gabbros. Associated cumulates plot as pyroxenite, a term not used here, given the lack of modal pyroxene in the rocks. Following a similar line of argument (lack of olivine), we prefer the term "gabbro" to "olivine gabbro".

The Primel cumulates mainly enclose labradorite, secondarily albitized, as a cumulus phase (from 30 to 65 vol. %), with interstitial actinolite (which replaces oikocrysts, probably of pyroxene), Fe-Ti oxides and apatite.

Pegmatoids are mainly composed of skeletal green hornblende and elongated albitized plagioclase. Relics of diopside have been identified in a few samples. Small comb-shaped Fe-Ti oxides, biotite and acicular apatite fill the spaces between the large crystals. The flecks of

243 the mottled pegmatoids on the western edge of Saint-Jean's bay contain Fe-Ti oxides,
244 amphibole and phyllosilicates. They might result from recrystallization of ancient oikocrystic
245 pyroxenes.
246 Gabbros and monzogabbros from the SJIC contain saussuritized plagioclase laths,
247 green hornblende, acicular actinolite, Fe-Ti oxides, apatite, biotite and sparse titanite and
248 zircon. Large oikocrysts of brown hornblende have been identified in several monzogabbro
249 samples. The dolerites are fine-grained and have a typical greenschist facies mineral
250 assemblage (albite, actinolite, epidote, chlorite).
251 The SJIC (Q-)monzonites are especially rich in andesine (up to 75 vol. %). The main
252 ferro-magnesian mineral is actinolite. The Q-monzonites, which are mainly located east of
253 Saint-Jean's bay, have more than 10 vol. % of quartz. Sheets and diapirs from the SJIC range
254 from diorite to Q-monzonite in composition. Sheets are rich in albitic plagioclase but also
255 contain amphibole (green hornblende and actinolite) with variable amounts of interstitial
256 quartz. Diapirs contain quartz, plagioclase, K-felspar and epidote.
257 Granites contain orthoclase, quartz, plagioclase, biotite, apatite and rare zircons.
258 Symplectitic quartz-feldspar associations are present in many SJIC granitic samples
259 (myrmekite).
260
261 **4. North-Guernsey Intrusive Complex (NGIC)**
262
263 *4.1. Geology*
264
265 Guernsey (Channel Islands), about 50 km off the French coast, is part of the
266 Armorican Massif (Fig. 1a). The island is divided into two main geological domains. The
267 Southern Metamorphic Complex mainly consists of Palaeoproterozoic gneisses (including the

268 Icart orthogneiss, with a magmatic U-Pb/zircon age of 2061 ± 2 Ma, Samson and D'Lemos,
269 1998), which were later intruded by the deformed Neoproterozoic Perelle Q-diorite (Samson
270 and D'Lemos, 1999). The Northern Neoproterozoic Intrusive Complex – hereafter referred to
271 as the North-Guernsey Intrusive Complex (NGIC) – is undeformed and partly composed of
272 layered rocks (Elwell et al., 1960, 1962; Bremond d'Ars, 1990; Bremond d'Ars et al., 1992).
273 The composite NGIC consists of four distinct units: the Saint Peter Port gabbro, the gabbro-
274 dioritic Bordeaux Group, the L'Ancresse granodiorite and the Cobo granite (Topley et al.,
275 1990; Fig. 1c). All these plutonic units were emplaced at the end of the Cadomian orogeny, at
276 about 560-550 Ma (Bremond d'Ars et al., 1992). The present study mainly deals with gabbro-
277 diorite layering in the Bordeaux Group (the Beaucette type in Bremond d'Ars et al., 1992) and
278 with the Spur Point cumulate-pegmatoid association (Saint Peter Port Gabbro). Alteration of
279 the NGIC rocks is generally moderate. Petrologic studies indicate that the Saint Peter Port
280 gabbro was emplaced under a lithostatic pressure of about 0.4 GPa (*c.* 12 km depth),
281 amphibole and plagioclase crystallized at about 940°C under relatively high oxygen fugacity
282 conditions, and magma water content ranged from 2 to 6 wt% (Bremond d'Ars et al., 1992).
283 The complex has a calc-alkaline affinity (Bremond d'Ars et al., 1992; see also section 5.2)
284 and belongs to the M-type Cadomian Granitoid Belt of Graviou and Auvray (1985).
285
286 *4.2. NGIC layering*
287
288 *4.2.1. Beaucette Marina: veined gabbroic macrorhythms*
289 The outcrops of the Beaucette Marina (gabbro-dioritic Bordeaux Group) show
290 partially cumulative macrorhythmic sequences, which are less than one to several meters
291 thick, and dip 20° westward (Fig. 2d, e and 5a, b, c). They are locally intruded by doleritic or
292 dioritic dykes. Each macrorhythm is composed of a gabbroic unit overlying a melagabbroic

293 unit. The base of a melagabbroic unit is generally fine-grained, as also observed by Elwell et
294 al. (1960). The transition from a melagabbroic unit to an overlying gabbroic one is
295 gradational, with amounts of phyric amphiboles decreasing upwards (see Fig. 9 insets in
296 section 5.1). Both units have an orthocumulate texture. While melagabbroic units are
297 petrologically homogeneous, the main gabbroic unit is formed by alternating dark and
298 mesocratic layers of a few centimeters thick (Fig. 5c) and is veined by leucocratic material,
299 forming an inter- and cross-connected network of centimeter-thick sheets, broadly parallel to
300 the layering (Fig. 5d).
301 Immediately below some melagabbroic units, thick evolved-gabbroic sheets are
302 observed, from which leucocratic pipes protrude upwards into the overlying melagabbros
303 (Fig. 5a, b). Such pipe-producing sheets also occur, more rarely, in the interior of the
304 melagabbroic units (Fig. 5a). They have a texture ranging from intergranular to
305 orthocumulative. The upper limit of the evolved-gabbroic sheets is irregular, sometimes
306 diffuse. Elwell et al. (1960) has described fine-grained margins in the upper part of some
307 gabbroic units at the contact with the pipe-producing sheets. All the leucocratic pipes are
308 inclined on average at about 30° from the main layering (Fig. 5e). They plunge toward the S-
309 SE. North of the area shown in Fig. 2e, two generations of neighboring pipes have distinct
310 pitches (*c.* 10° and 40° from the layering). Pipe compositions range from monzodiorite (this
311 study) to granodiorite (Elwell et al., 1960). In cross-section, the pipes are zoned, the core
312 being less differentiated than the rim (Fig. 5f; Elwell et al., 1960). The upper part of the pipes
313 is pegmatitic and the host rocks are systematically altered near the pegmatitic zones (Fig. 5f).
314 Elwell et al. (1960) have described two spots where pipes join with the overlying cross-
315 connected dioritic vein system.
316
317 *4.2.2. Spur Point: cumulate-pegmatoid association*

318 The Saint Peter Port gabbro is a 0.8 km-thick layered slab, gently dipping westward
319 (Briden et al., 1982). It is composed of three main rock types (Bremond d'Ars et al., 1992).
320 The most spectacular of which is the mottled orthocumulate of Spur Point, characterized by
321 layers of poikilitic amphibole crystal flecks (Roach, 1971; Bremond d'Ars, 1990; Bremond
322 d'Ars et al, 1992; Fig. 6a, b). This facies has been interpreted as a boundary layer cumulate
323 (Bremond d'Ars et al, 1992).
324 Pegmatoidic rocks crop out at Spur Point (Fig. 6c). Their mineralogy and texture are
325 similar to those in the SJIC. However, here in the NGIC, cumulates associated with
326 pegmatoids are mottled.
327
328 *4.3. Petrology*
329
330 In a R1-R2 diagram (La Roche et al., 1980), Beaucette's rocks are gabbronorite
331 (melagabbroic units), olivine gabbro (gabbroic units and pipe-producing sheets), diorite
332 (dykes and cross-connected veins), and monzodiorite (pipes). As for Primel (SJIC), the Spur
333 Point cumulates plot as pyroxenite, a term not used here.
334 The Spur Point mottled orthocumulates contain cumulus calcic plagioclase (An 80)
335 and clinopyroxene (Fig. 6b). The intercumulus phases are clino- and orthopyroxene,
336 amphibole (hastingsite), Fe-Ti oxides and apatite. The flecks correspond to large oikocrystic
337 amphiboles.
338 The NGIC pegmatoids are composed of large skeletal green hornblende, elongate
339 albitized plagioclase, comb-shaped Fe-Ti oxides, biotite and acicular apatite.
340 Gabbroic and granitic rocks have also mineralogies comparable to those of the SJIC
341 gabbros and granites. The melagabbros (gabbronorites) show green hornblende as cumulus

342 phase (< 50 vol. %), as well as plagioclase, Fe-Ti oxides, apatite and biotite. We have also
343 noted the presence of clots of small amphibole grains in these rocks.
344 In Beaucette, the dioritic veins, sheets and dykes are mainly composed of plagioclase,
345 hornblende and biotite, whereas the monzo/granodioritic pipes are rich in plagioclase, K-
346 felspar, green hornblende and, occasionally, quartz and clinopyroxene. The sheet sample
347 GS13a is composed of *c.* 30 % of 2 mm-long zoned plagioclase, as cumulus phase.
348 Concentrations of acicular hornblende are observed where pipes connect overlying cross-
349 connected dioritic veins (Elwell et al., 1960).
350 The pipe-producing evolved gabbroic sheet sample GS13a from Beaucette and the
351 mottled orthocumulate sample GS1a from Spur Point are both characterized by cumulus An-
352 rich plagioclase (An 60-90: Fig. 7a). No other analyzed NGIC sample shows such a
353 characteristic. A chemical profile across such a plagioclase crystal (sample GS1a, Fig. 7b)
354 reveals a calcic mantle (An 60-75) comprised between an An-rich core (An 75-90) and an An-
355 poor margin (An 40-55). This mineralogical specificity will be discussed in section 6.3.1.
356
357 **5. Geochemistry**
358
359 *5.1. Geochemical sections through gabbro-diorite units*
360
361 Vertical variations of MgO, TiO_2 and Al_2O_3 through four gabbro-dioritic sections are
362 shown in Figs 8 (SJIC) and 9 (NGIC). The chemical composition of the Poul Rodou gabbro is
363 relatively constant, above and below the diapir-producing leucocratic sheets, for all the
364 sections (Fig. 8). Only TiO_2 varies significantly, from 1.18 (SJ34g) to 1.91 wt% (SJ43f). This
365 relative chemical homogeneity of the mafic body is a rather original feature with respect to
366 many other MASLIs (e.g., Wiebe, 1996). By contrast, the macrorhythmic sequences of the

NGIC display variable compositions (Fig. 9). Melagabbros are highly magnesian, with MgO contents up to 14.35 wt% (GS10d). MgO is slightly higher in the lower part of the melagabbroic units (GS7a versus GS7d in Fig. 9). Gabbroic units are more heterogeneous and less magnesian (5 < MgO < 10 wt%, Fig. 9). The leucocratic veins, sheets and diapirs/pipes display various compositions. In both intrusions, the diapirs/pipes are systematically more evolved than the sheets from which they are extracted (SJ34b1 versus SJ34c; GS10c versus GS13a; Table 1 and Figs 8 and 9). However, parts of some sheets are more differentiated than some diapirs. For example, the upper part of the sheet SJ43c is more evolved than the diapir SJ34b1, which relates to another sheet (Table 1 and Fig. 8).

5.2. Trace elements

Trace elements which are both incompatible and immobile can be used to determine the magmatic affinity of the mafic rocks. In the La/10-Y/15-Nb/8 diagram (Fig. 10) of Cabanis and Lecolle (1989), the SJIC gabbros and monzogabbros plot mainly in the E-MORB field whereas the gabbros and melagabbros from the NGIC clearly have a calc-alkaline affinity.

The chondrite-normalized rare earth element (REE) field of the Poul Rodou gabbros (SJIC) is shown in Fig. 11a, with REE patterns of two leucocratic sheets and related diapirs. The sheet and diapir SJ34 are moderately differentiated. The diapir SJ34b1 is slightly enriched in light REE (LREE) and depleted in heavy REE (HREE) with respect to the corresponding sheet SJ34c, which plots above the gabbroic field. The sheet sample SJ43c shows lower REE concentrations than the less differentiated sheet sample SJ34c. The diapir SJ43d is enriched in LREE and depleted in HREE with respect to its parental sheet SJ43c. Both have positive Eu anomalies.

392 The REE patterns of some other rocks representative of the SJIC are exhibited in Fig.
393 11b. Pattern similarities between the diapir SJ34b1 and the monzonite SJ9 (mingling zone at
394 Saint-Jean's bay) and between the evolved sheet SJ43c and the Q-monzonite SJ17 (vein in
395 breccia with angular clasts at Saint-Jean's bay) are noticeable. The pegmatoid SJ16 is less rich
396 in REE than the gabbros. Of all the samples, cumulates have the lowest REE contents. With
397 respect to the monzonite SJ9, the granite SJ22 is enriched in Ce and HREE, and displays a
398 large negative Eu anomaly.
399 In the NGIC, all the samples from the macrorhythmic sequences have parallel patterns
400 (Fig. 11c). This is also the case for the pipe-producing gabbroic sheet GS13a, located near the
401 upper limit of the gabbroic REE field. By contrast, the thin dioritic sheet GS7c and the
402 monzodioritic pipe GS10c are highly depleted in HREE with respect to GS13a. Although
403 contents of La, Eu and Yb are equal in GS10c and GS7c, GS10c has a concave-up shaped
404 pattern indicating depletion in Middle REE (with the exception of Eu).
405 The gabbroic pipe-producing sheet GS13a and the mottled cumulate of Spur Point
406 GS1a, which contain An-rich plagioclase phenocrysts (An 60-90: Fig. 7), display cross-
407 cutting REE curves, with comparable Eu contents (Fig. 11d). The Cobo granite GS8 has a
408 concave-up pattern and a negative Eu anomaly.
409
410 *5.3. Isotopes*
411
412 The Sr and Nd isotopic data and analytic details are shown in Table 2. The range of
413 the NGIC $^{87}Sr/^{86}Sr$ initial ratios is very restricted (0.7055 to 0.7058), regardless of the rock
414 type (data from Bremond d'Ars et al., 1992). In the SJIC, mafic rocks (gabbros, pegmatoids,
415 and dolerites) exhibit the most positive εt_{Nd} values at 347 Ma (+4.7 to 5.9) and initial Sr ratios
416 between 0.7039 and 0.7049. These values are similar to those obtained by Barboni et al.

417 (2010) on pseudo-adakites related to the SJIC (+2.9 to + 6.8 and 0.7038 to 0.7047). The
418 intermediate SJIC rocks (monzogabbros, monzonites, Q-monzonites, and diorite) have less
419 positive εt_{Nd} values (+2.4 to +3.2) and initial Sr ratios which range from 0.7043 to 0.7069.
420 This scattering suggests that the Rb-Sr system was not closed. The granite sample SJ22 also
421 exhibits a positive εt_{Nd} value at 347 Ma (+3.0) and a low initial Sr ratio (<0.700) which also
422 shows open system behavior for Rb-Sr. A noticeable feature is the sharp isotopic contrast
423 between the Poul Rodou gabbro SJ34a (+5.9) and the dioritic sheet SJ34c (+2.6), two
424 neighbor samples separated by *c.* 3 m (Fig. 3a and 8).
425 It follows that the gabbro and the leucocratic sheets from Poul Rodou are not
426 cogenetic. The source of the former corresponds to that of the doleritic dykes and peripheral
427 pegmatoids, whereas the Poul Rodou sheets (and diapirs) have an isotopic composition
428 comparable to that of the other SJIC intermediate rocks.
429
430 **6. Discussion**
431
432 *6.1. A review*
433
434 *6.1.1. MASLI-type reservoirs: the models*
435 Wiebe and others have defined the concept of MASLI and studied many examples of
436 such intrusions, especially in Maine. A MASLI petrologically corresponds to a composite
437 layered sequence of alternating gabbroic and dioritic units situated between or below granitic
438 bodies (Chapman and Rhodes, 1992; Wiebe, 1996; Wiebe and Collins, 1998). Variants are
439 intrusions of bimodal gabbro-diorite (e.g., Ingonish, Cape Breton Island: Wiebe, 1974) or
440 diorite-granite (e.g., Nord-Forez, Massif Central, France: Barbarin, 1988), which display
441 some of the characteristic features of MASLIs. These complexes are interpreted to be the

442 result of repeated mafic intrusions in a crystallizing dioritic/granitic reservoir (Wiebe, 1974,
443 1993b, 1996). This group of models is supported, among other things, by the observation of
444 pillow-like bodies of chilled gabbro in intermediate/felsic rocks (Wiebe, 1993b; Wiebe et al.,
445 2001). Diorites are generally viewed either as products of fractional crystallization of the
446 gabbro, or as resident cumulates.

447 A multistep model for the Isle au Haut Maine igneous complex (Maine), similar to
448 those of Wiebe and others, was proposed by Chapman and Rhodes (1992). The model
449 accounts for the formation of a layered sequence of ten alternating (tholeiitic) gabbroic and
450 dioritic units of magmas, which were contemporaneous. The bases of the gabbros are chilled
451 against the underlying diorites. The authors state that mafic liquids were periodically
452 emplaced into a silicic magma chamber at the rheological transition from a relatively felsic
453 cumulate to an overlying felsic magma. Each gabbroic unit is injected below a dioritic liquid,
454 but above a solidifying dioritic crystal mush, as expected from the magma density contrast.
455 Once emplaced, crystallization progresses in the underlying dioritic mush and produces Q-
456 monzodioritic sheets and pipes, which intrude the gabbroic layer. Diapirs are subsequently
457 produced from the crystallizing sheets.

458 The development of such gravity-driven instabilities in layered magmas have been
459 modeled and applied to the NGIC (Bremond d'Ars, 1990; Bremond d'Ars and Davy, 1991).
460 However, according to these authors, it is not clear whether the sheets in the NGIC result
461 from intrusions within the gabbros, or the reverse. The opinion of Wiebe (1993b) is that "the
462 'veins' in Guernsey have textures and compositions that are appropriate for feldspar
463 cumulates, not solidified liquids". He views the NGIC as a crystallizing intermediate/felsic
464 reservoir periodically invaded by mafic liquids.

465

466 *6.1.2. Cumulates and pegmatoids*

467 The connection between mafic cumulates, gabbroic pegmatites (pegmatoids) and
468 aplites has been established by many authors. For instance, Beard and Day (1986) published a
469 thorough study of such rocks in the Smartville intrusive complex, Sierra Nevada, California.
470 They pointed out the following features: (i) the pegmatoids occur as pods and segregations in
471 gabbroic rocks; (ii) they are often found in association with fine-grained aplite of similar
472 mineral assemblage; and (iii) they have a very mafic composition, as observed by other
473 authors (e.g., McBirney and Noyes, 1979). Contrary to previous authors who proposed
474 subsolidus processes (e.g., Bow et al., 1982), Beard and Day (1986) favour that rocks form by
475 *in situ* crystallization. They envisage that a mafic intercumulus melt is extracted from a
476 cumulate stack in the presence of a fluid phase. The process could be enhanced by the
477 disruption of the cumulate assemblage due to a drop in the confining pressure. This model is
478 consistent with the one proposed by Momme and Wilson (2002) for the Kraemer Island
479 macrodyke, Greenland. It is also similar to the model of pegmatoid formation in thick basaltic
480 lava flows proposed by Caroff et al. (1997). An alternative model suggests that the pegmatoid
481 crystals grew by reaction between primary mafic mineral grains and a superheated liquid
482 possibly resulting from a pressure drop (Cawthorn and Boerst, 2006). In a plumbing system
483 connected to the surface, a pressure drop can easily be achieved subsequent to an eruption. In
484 an intrusion, confined at depth within deformable host rocks, only a volumetric expansion of a
485 constant mass plumbing system could also induce a pressure drop.
486
487 *6.2. Layering and diapirism in the SJIC and NGIC*
488
489 Both SJIC and NGIC display comparable characteristics, which justifies the present
490 combined study: (1) both intrusions are triple-component MASLIs (gabbro, diorite and
491 granite); (2) pegmatoids occur in association with mafic cumulates, especially at the edges of

492 both complexes; (3) a lateral or basal part of the intrusions is formed by gabbroic sequences
493 interlayered with dioritic sheets producing diapirs. Nevertheless, numerous contrasted features
494 lead us to propose two different models for the construction of the gabbro-dioritic layered
495 sequences.
496
497 *6.2.1. Melagabbros and gabbros*
498 Two noticeable features of the NGIC gabbro-dioritic unit not observed in the SJIC are
499 the presence of macrorhythms and modal layering within the gabbroic sequences. This
500 petrological heterogeneity induces geochemical variations (Fig. 9 and 11c) and suggests
501 crystal accumulation. By contrast, the tholeiitic Poul Rodou gabbro (SJIC) is relatively
502 homogeneous (Fig. 11a). Therefore, it is probably not a cumulate, but was rather a liquid that
503 crystallized *in situ* without significant crystal settling, possibly after a period of convection.
504 For instance, Philpotts et al. (1996) have shown that tholeiitic magmas, when only one-third
505 crystallized, can form crystal mushes dominated by thin laths of plagioclase and elongated
506 pyroxene grains. In such magmas, an interlocking network of crystals can form at low solid
507 content (possibly only 20%), precluding any further convection and crystal settling. Such a
508 model is consistent with both the tholeiitic affinity of the Saint-Jean gabbro (Fig. 10) and the
509 rock textures, which are intergranular to oikocrystic. On the contrary, the rhythmic sequences
510 of the calc-alkaline NGIC, and the orthocumulate texture fit with a crystal accumulation
511 model.
512 In Fig. 12, we propose two models to explain the formation of the gabbro-dioritic
513 layered sections of the SJIC and NGIC. The Poul Rodou gabbro is purported to be a simple
514 network-type crystal mush, crystallizing from the base up (Fig. 12a, b, c). In Beaucette, each
515 melagabbro/gabbro pair is asserted to correspond to a mafic recharge (Fig. 12d, g), having
516 undergone two successive crystal-settling events. At first, settling involves only mafic crystals

517 (olivine, pyroxene ± primary hornblende: Fig. 12e) and next, plagioclase appears on the
518 liquidus (Fig. 12f). In the first step, densities of the mafic crystals are comparable and the
519 resulting cumulate is highly mafic and texturally homogeneous (melagabbroic unit). With the
520 appearance of plagioclase, the density difference between feldspar and mafic crystals can
521 produce alternating dark/mesocratic layers (gabbroic unit), according to the model of Sparks
522 et al. (1993).
523
524 *6.2.2. Formation of leucocratic sheets and diapirs*
525 Models of dioritic/monzonitic reservoirs periodically replenished by mafic liquids
526 hardly apply to all the stages of construction of both intrusions.
527 *In the SJIC*, observations supporting the idea that intermediate magmas have invaded
528 mafic ones include: (1) the several sheets of intermediate composition that we interpret as
529 intrusions in the Poul Rodou homogeneous gabbro; (2) the monzonitic dykes throughout most
530 of Saint-Jean's bay, especially those including angular mafic breccias (Fig. 4c); (3) the lack of
531 evidence for chilling of the Poul Rodou gabbro against the dioritic sheets (Fig. 8); and (4) the
532 large predominance of the gabbroic rocks over the whole intrusion. We do not exclude that
533 mafic inputs, at huge rates, possibly inducing intensive thermal rejuvenation of a more felsic
534 resident magma, were previously involved in the SJIC. We mean here that, as observed today,
535 (1) and (2) are unlikely the direct, *in situ* or slightly displaced, remnants of an initial felsic
536 reservoir that remains rather hypothetical from (3) and (4).
537 The chilled gabbroic pillow-like enclaves, such as those of Fig. 4a, result from
538 fragmentation of mafic magmas in more felsic ones. Such a mingling is controlled by
539 rheological contrasts and/or surface energy and depends on the relative volumes and
540 temperatures of available magmas (e.g., Sparks and Marshall, 1986; Fernandez and Barbarin,
541 1991; Hallot et al., 1996; Pons et al., 2006). Thus, it can be achieved during or just after new

542 mafic inputs, but may alternatively result from convective motions in the interior of a large
543 composite reservoir or from injections of an external more felsic magma into a resident mafic
544 magma. Chilling of the latter just requires significant volumes of colder, but still mobile,
545 more felsic magmas.

546 Therefore, we propose a model of a reservoir repeatedly replenished by dioritic
547 magmas for the SJIC. Those magmas were not genetically related, nor had they to be initially
548 at the same temperature. In the reservoir, the gabbroic magma density increases downward
549 with cooling, hence crystallinity. Andesites/diorites and basalts/gabbros may have comparable
550 densities, especially when they are of tholeiitic affinity (e.g., Sparks et al., 1980; Sparks and
551 Huppert, 1984; Caroff, 1995). A partly crystallized dioritic magma rising through a tholeiitic
552 gabbro crystallizing from below is thus expected to be buoyant initially, then at neutral
553 buoyancy and finally denser than the gabbroic magma. In Fig 12a and b, a 950°C dioritic
554 magma with 30% plagioclase phenocrysts enters a gabbroic reservoir crystallizing from
555 below. At the base (1), the gabbroic magma is 70% solid at 1100°C. At upper levels (2) and
556 (3), it is 30% solid at 1150°C and liquid at 1200°C, respectively (all values are approximates).
557 Reaction kinetics being much slower than heat transfer, a metastable dioritic melt plus
558 crystals at thermal equilibrium with the resident magma is considered at these levels.
559 Densities were estimated given that the density of a liquid, obtained from Bottinga and Weill
560 (1970), is about 90% of that of its solid equivalent and assuming that this ratio applies to the
561 solid fraction whatever it is (Fig. 12). The results show that at levels (1) and (2), a gabbroic
562 magma remains denser than a dioritic magma. At level (3), equidensity is reached allowing a
563 dioritic magma to spread out, forming sheets. Thus, we interpret each SJIC sheet as the result
564 of some horizontal emplacement of porphyric magmas of intermediate composition into
565 poorly crystallized gabbros at levels of neutral buoyancy. Late felsic diapirs formed at the top
566 of emplaced sheets while the equidensity front moved upward as cooling proceeded (Fig. 12b

567 and c). *In situ* fractionation within the sheets favored the late production of low density
568 magmatic liquids. The REE patterns of the diapirs are depleted in HREE with respect to the
569 sheets from which they were extracted (Fig. 11a). This is consistent with fractionation of a
570 significant amount of amphibole within the sheets. Indeed, amphibole preferentially
571 incorporates middle to heavy REE relative to LREE (e.g., Caroff et al., 1999).
572 *In the NGIC*, dioritic sheet and vein geometries are controlled by the macrorhythms:
573 the pipe-producing sheets are generally located along the lower boundary of the melagabbroic
574 units and the cross-connected dioritic vein network forms in the gabbroic units according to
575 the framework of the dark/mesocratic layers. These features suggest that the gabbroic
576 structures existed prior to the dioritic veining. The fine-grained margins at the base of
577 melagabbroic units relate to mafic replenishments before the dioritic invasion.
578 The main similarity between the SJIC and the NGIC was the late influx of the dioritic
579 magmas with respect to the main gabbroic magmas. At Beaucette, both magmas were close to
580 isotopic equilibrium. The emplacement of the dioritic sheets was not directly controlled by
581 density ratios, but rather by pre-existent rhythmic structures within cumulates (Fig. 12h). Two
582 groups of sheets have to be distinguished. An initial gabbroic to dioritic magma was emplaced
583 just beneath the base of the melagabbroic units (Fig. 5a, c). The sheet-derived pipes cut across
584 the melagabbroic unit (Fig. 5b), until the overlying gabbroic unit. The concave-up shape of
585 the REE pattern of the pipe GS10c (Fig. 11c) is consistent with crystallization and
586 fractionation of both amphibole and apatite in its parental sheet (Caroff et al., 1999). Relative
587 motions between the unconsolidated/mushy units possibly caused the vertical pipes to become
588 inclined (Fig. 5e, 12i), as previously proposed by Elwell et al. (1960). They might have
589 created proto-fissures in the gabbroic unit and thus have favored the emplacement of the
590 (monzo)dioritic second group of sheets, which are cross-connected and fed by the pipes (Fig.
591 5d, 12i). The gabbroic layering, seen as controlling the architecture of the cross-connected

592 vein/sheet network, supports our interpretation of late dioritic invasion within gabbros.
593 Cumulative features of the sheets reveal that the invading magmas possibly contained
594 plagioclase phenocrysts, such as those in the SJIC.
595
596 *6.3. Variations in the mode of MASLI construction*
597
598 Our models (Fig. 12) agree with the general physical conditions and the mechanisms
599 by which layers, pipes, diapirs and other plutonic structures are supposed to form within
600 crystallizing magmas (e.g., see Barbey, 2009 and Patterson, 2009 and references therein for
601 recent reviews). In our opinion, the SJIC and the NGIC support the general idea that
602 intermediate/felsic replenishment of a mafic reservoir is a situation much more common than
603 previously thought, though not as common as mafic replenishment.
604
605 *6.3.1. NGIC*
606 Bremond d'Ars et al. (1992) have proposed a sketchy model of the NGIC reservoir.
607 According to these authors, the layered rocks (Saint-Peter Port cumulate and Beaucette-type
608 gabbro-diorite) formed near the margin of the chamber, by upwards prograding crystallization
609 and replenishments. The present dip of the layers is primary. Far from the margins, the centre
610 of the reservoir was probably convective, which explains the lack of layering in most of the
611 Bordeaux gabbro-diorite outcrops, with the exception of Beaucette. The peripheral granitic
612 bodies (Cobo, L'Ancresse) are proposed to form by mixing and assimilation of crust-derived
613 melts with the gabbro-diorite magmas. Large volumes of mafic magma are thought to have
614 induced melting of country rocks at depth within the plumbing system.
615 We agree with the basic ideas of this model, except for the the hypothesis of crustal
616 melting. Although interactions between gabbro-dioritic and granitic rocks are undeniable

617 (Topley et al., 1982; D'Lemos, 1996), available isotopic data seems hardly consistent with
618 crustal melting (Table 2). We rather suggest, as D'Lemos (1996), that at least the Cobo
619 granite is to a great extent cogenetic with the Bordeaux gabbro-diorite, as it is often observed
620 in MASLIs (e.g., Wiebe, 1993a, b, 1994, 1996; Wiebe and Collins, 1998).
621 An-rich plagioclases in both the mottled cumulate GS1a from Spur Point and the
622 gabbroic sheet sample GS13a from Beaucette support the hypothesis that the invading dioritic
623 liquid(s) originate(s) from the mottled Saint-Peter-Port/Spur Point cumulate, interpreted as a
624 boundary layer by Bremond d'Ars et al. (1992). An-rich plagioclase cores (An>75, Fig. 7b)
625 suggest crystallization under hydrous conditions (Cordier et al., 2007). Derivation of a
626 GS13a-type composition from a liquid leaving a GS1a-type cumulate is also supported by
627 trace element compositions. Indeed, cross-cutting REE curves in Fig. 11d possibly reflect
628 crystal fractionation/accumulation (plagioclase, amphibole and/or apatite).
629
630 *6.3.2. SJIC*
631 A model of the SJIC is drawn in Fig. 13.
632 Granitic intrusions (Fig. 2a) have emplaced during or just after the crystallization of
633 the gabbro-dioritic magmas.
634 Pegmatoids and associated mafic cumulates are located near the edge of the complex
635 (Fig. 1b and 2b, c). With an isotopic composition close to that of the Poul Rodou gabbro and
636 the doleritic dykes, but more mafic, pegmatoids likely correspond to liquids issued from a
637 mafic intercumulus melt in the presence of a fluid phase. Melt extraction might have been
638 enhanced by the disruption of the cumulate stack, perhaps in a context of drop of the
639 confining pressure (Beard and Day, 1986; Momme and Wilson, 2002). Reactions of the liquid
640 with primary mafic minerals of the cumulate might explain Mg-rich pegmatoid compositions
641 (Cawthorn and Boerst, 2006).

642 Mixing and mingling seem to have preferentially occurred in the central part of the
643 reservoir. Dioritic liquids (in a broad sense) mix with gabbroic magmas to form variable
644 hybridized products, the isotopic composition of which tends toward that of the diorites. The
645 most homogeneous hybridized product, which has a dioritic isotopic signature (Table 2),
646 corresponds to the Saint-Jean's bay monzogabbro. Such an isotopic homogenization in a
647 MASLI, by mixing and diffusion (Steward and De Paolo, 1992), has already been described
648 by Waight et al. (2007). Angular breccias, also drawn in Fig. 13, can result either from
649 gabbro/diorite interactions in a more peripheral (i.e. colder) region of the reservoir, or,
650 alternatively, from late arrivals of dioritic liquids in a solidifying magma. The ductile to brittle
651 behavior of a magma which can be inferred from the preserved shapes of the enclaves also
652 depends on the strain rates involved during fragmentation (Fernandez and Gasquet, 1994;
653 Hallot et al., 1996; Petford, 2009).
654 At Poul Rodou, the isotopic composition of the felsic sheets differs from that of the
655 enclosing resident gabbro. The SJIC intermediate and felsic products are therefore issued
656 from a source which is different from that of the Poul Rodou gabbro / Primel pegmatoid /
657 Saint-Jean dolerite group. An AFC-type crustal contamination of the felsic liquid in a deep
658 reservoir possibly accounts for such features.
659
660 **7. Conclusions**
661
662 (1) The Saint-Jean-du-Doigt (SJIC) and the North-Guernsey (NGIC) Intrusive
663 Complexes are two MAfic-Silicic Layered Intrusions (MASLI) of the armorican Massif. Both
664 are triple component complexes (gabbro, diorite, granite) characterized by the occurrence of
665 pegmatoids in association with cumulates and of gabbroic units including diapir-producing

dioritic sheets. The NGIC is Cadomian and calc-alkaline. Mafic rocks of the Hercynian SJIC are tholeiitic.

(2) Pegmatoids are interpreted as liquids extracted from a mafic intercumulus melt in the presence of a fluid phase, subsequent to the disruption of a peripheral cumulate stack, possibly during a drop of the confining pressure.

(3) At least at some stages, the gabbro-dioritic units of the SJIC and the NGIC can both result from repeated influxes of magmas of intermediate composition within mafic reservoirs, but they are built differently. The SJIC gabbro could result from *in situ* crystallization of a relatively uniform magma in which crystal settling was not significant. Assuming they were metastable, dioritic magmas could have risen as gravity-driven diapirs in such a crystallizing gabbro before they spread to form sheets at levels of neutral buoyancy. By contrast, the NGIC gabbros correspond to cumulates. At Beaucette, they display a rhythmic layering which has guided the subsequent dioritic injections.

Acknowledgements

We are grateful to P.-M. Le Dantec for field assistance (Primel and Roc'h Louet cartography). Detailed and constructive comments by Dr P. Barbey and an anonymous reviewer helped us to improve the manuscript. Pertinent suggestions of A. Brink are gratefully acknowledged. We also thank Dr C.G. Barnes for discussions and Dr N. Eby for editorial assistance.

References

689 Auvray, B., Charlot, R., Vidal, P., 1980. Données nouvelles sur le protérozoïque inférieur du
690 domaine nord-armoricain (France) : âge et signification. Canadian Journal of Earth
691 Sciences 17, 532-538.
692 Barbarin, B., 1988. Field evidence for successive mixing and mingling between the Piolard
693 Diorite and the Saint-Julien-la-Vêtre Monzogranite (Nord-Forez, Massif Central,
694 France). Canadian Journal of Earth Sciences 25, 49-59.
695 Barbey, P., 2009. Layering and schlieren in granitoids: a record of interactions between
696 magma emplacement, crystallization and deformation in growing plutons. Geologica
697 Belgica 12, 109-133.
698 Barboni, M., Bussy, F., Schoene, B., Schaltegger, U., 2008. Architecture and emplacement
699 mechanism of the Saint Jean du Doigt bimodal intrusion, Brittany, France. Geophys.
700 Res. Abstr. 10, EGU2008-A-05182.
701 Barboni, M., Bussy, F., Chiaradia, M., 2010. Origin of Early Carboniferous pseudo-adakites
702 in northern Brittany (France) through massive amphibole fractionation from hydrous
703 basalt. Terra Nova, doi:10.1111/j.1365-3121.2010.00974.x.
704 Beard, J.S., Day, H.W., 1986. Origin of gabbro pegmatite in the Smartville intrusive
705 complexe, northern Sierra Nevada, California. American Mineralogist 71, 1085-1099.
706 Bottinga, Y., Weill, F., 1970. Densities of liquid silicate systems calculated from partial molar
707 volumes of oxide components. American Journal of Science 269, 169-182.
708 Bow, C., Wolfgram, D., Turner, A., Barnes, S., Evans, J., Zdepski, M., Boudreau, A., 1982.
709 Investigations of the Howland reef of the Stillwater Complex, Minneapolis adit area :
710 stratigraphy, structure, and mineralization. Economic Geology 77, 1481-1492.
711 Bremond d'Ars, J. de, 1990. Estimation des propriétés rhéologiques des magmas par l'étude
712 des instabilités gravitaires. Pétrologie du complexe plutonique de Guernesey. Mémoires

et Documents du Centre Armoricain d'Etude Structurale des Socles (Thesis), Rennes 35, 370 p.

Bremond d'Ars, J. de, Davy, P., 1991. Gravity instabilities in magma chambers – rheological modeling. Earth and Planetary Science Letters 105, 319-329.

Bremond d'Ars, J. de, Martin, H., Auvray, B., Lécuyer, C., 1992. Petrology of a magma chamber: the plutonic complex of Guernsey (Channel Islands, UK). Journal of the Geological Society of London 149, 701-708.

Briden, J.C., Clark, A., Fairhead, J.D., 1982. Gravity and magnetic studies in the Channel Islands. Journal of the Geological Society of London 139, 35-48.

Cabanis, B., Lecolle, M., 1989. Le diagramme La/10-Y/15-Nb/8: un outil pour la discrimination des séries volcaniques et la mise en évidence des processus de mélange et/ou de contamination crustale. Comptes Rendus de l'Académie des Sciences de Paris 309, série II, 2023-2029.

Capdevila, R., 2010. Les granites varisques du Massif armoricain. Bulletin de la Société Géologique et Minéralogique de Bretagne (D) 7, 1-52.

Caroff, 1995. Open system crystallization and mixing in two-layer magma chambers. Lithos 36, 85-102.

Caroff, M., Ambrics, C., Maury, R.C., Cotten, J., 1997. From alkali basalt to phonolite in handsize samples: vapor-differentiation effects in the Bouzentès lava flow (Cantal, France). Journal of Volcanology and Geothermal Research 79, 47-61.

Caroff, M., Guillou, H., Lamiaux, M., Maury, R.C., Guille, G., Cotten, J., 1999. Assimilation of ocean crust by hawaiitic and mugearitic magmas: an example from Eiao (Marquesas). Lithos 46, 235-258.

Cawthorn, R.G., Boerst, K., 2006. Origin of the pegmatitic pyroxenite in the Merensky Unit, Bushveld Complex, South Africa. Journal of Petrology 47, 1509-1530.

738 Chantraine, J., Chauris, L., Cabanis, B., Chauris, M.-M., Larsonneur, C., Herrouin, Y., Rabu,
739 D., Lulzac, Y., Bos, P., 1986. Notice explicative, carte géol. France (1/50 000), feuille
740 Plestin-Les-Grèves (202). Orléans, BRGM, 84 p. Geological map by J. Chantraine *et al.*
741 (1985).
742 Chapman, M., Rhodes, J.M., 1992. Composite layering in the Isle au Haut Maine igneous
743 complex, Maine: Evidence for periodic invasion of a mafic magma into an evolving
744 magma reservoir. Journal of Volcanology and Geothermal Research 51, 41-60.
745 Coint, N., Caroff, M., Hallot, E., Peucat, J.J., 2009. The gabbro-diorite layered intrusions of
746 Saint-Jean-du-Doigt (France) and Beaucette (Guernsey, Channel Island), Armorican
747 Massif: an emplacement model. Geological Society of America Abstracts with
748 Programs 41 (2), 30.
749 Coint, N., Hamelin, C., Caroff, M., 2008. Le complexe gabbro-dioritique lité de Saint-Jean-
750 du-Doigt, Massif armoricain: un exemple de réservoir magmatique de type MASLI.
751 Bulletin de la Société Géologique et Minéralogique de Bretagne (D) 5, 1-29.
752 Collins, W.J., Wiebe, R.A., Healy, B., Richards, S.W., 2006. Replenishment, crystal
753 accumulation and floor aggradation in the megacrystic Kameruka suite, Australia.
754 Journal of Petrology 47, 2073-2104.
755 Cordier, C., Caroff, M., Juteau, T., Fleutelot, C., Hémond, C., Drouin, M., Cotten, J.,
756 Bollinger, C., 2007. Bulk-rock geochemistry and plagioclase zoning in lavas exposed
757 along the northern flank of the Western Blanco Depression (Northeast Pacific): Insight
758 into open-system magma chamber processes. Lithos 99, 289-311.
759 Cotten, J., Le Dez, A., Bau, M., Caroff, M., Maury, R., Dulski, P., Fourcade, S., Bohn, M.,
760 Brousse, R., 1995. Origin of anomalous rare-earth element and yttrium enrichments in
761 subaerial exposed basalts: Evidence from French Polynesia. Chemical Geology 119,
762 115-138.

763 De Paolo, D.J., 1988. Neodymium isotope geochemistry, an introduction. Mineral and rocks,
764 20. Springer Verlag, Berlin, Heidelberg.
765 D'Lemos, R.S., 1996. Mixing between granitic and dioritic crystal mushes, Guernsey,
766 Channel Islands, UK. Lithos 38, 233-257.
767 Elwell, R.W.D., Skelhorn, R.R., Drysdall, A.R., 1960. Inclined granitic pipes in the diorites of
768 Guernsey. Geological Magazine 97, 89-105.
769 Elwell, R.W.D., Skelhorn, R.R., Drysdall, A.R., 1962. Net veining in the diorite of north east
770 Guernsey, Channel Islands. Journal of Geology 70, 215-226.
771 Fernandez, A.N., Barbarin, B., 1991. Relative rheology of coeval mafic and felsic magmas :
772 Nature of resulting interaction processes and shape and mineral fabrics of mafic
773 microgranular enclaves. In: Didier, J., Barbarin, B. (Eds), Enclaves and granite
774 petrology. Elsevier, Amsterdam, p. 263-275.
775 Fernandez, A.N., Gasquet, D.R., 1994. Relative rheological evolution of chemically
776 contrasted coeval magmas: example of the Tichka plutonic complex (Morocco).
777 Contributions to Mineralogy and Petrology 116, 316-326.
778 Franceschelli, M., Puxeddu, M., Cruciani, G., Dini, A., Loi, M., 2005. Layered amphibolite
779 sequence in NE Sardinia, Italy : remnant of a pre-Variscan mafic silicic layered
780 intrusion ? Contributions to Mineralogy and Petrology 149, 164-180.
781 Graviou, P, Auvray, B., 1985. Caractérisation pétrographique et géochimique des granitoïdes
782 cadomiens du domaine nord-armoricain: implications géodynamiques. Comptes Rendus
783 de l'Académie des Sciences de Paris 301, 315-318.
784 Hallot, E., Davy P., Bremond d'Ars J. de, Auvray, B., Martin H., Van Damme H., 1996. Non-
785 newtonian effects during injection in partially crystallized magmas. Journal of
786 Volcanology and Geothermal Research 71, 31-44.

787 Hellström, F.A., Johansson, A., Larson, S.A., 2004. Age and emplacement of late
788 Sveconorwegian monzogabbroic dykes, SW Sweden. Precambrian Research 128, 39-55.
789 Johnson, M.C., Rutherford, M.J., 1989. Experimental calibration of the aluminium-in-
790 hornblende geobarometer with application to Long Valley caldera (California) volcanic
791 rocks. Geology 17, 837-841.
792 La Roche, H. de, Leterrier, J., Grandeclaude, P., Marchal, M., 1980. A classification of
793 volcanic and plutonic rocks using R1R2-diagrams and major-element analyses – its
794 relationships with current nomenclature. Chemical Geology 29, 183-210.
795 López-Moro, F.J., López-Plaza, M., 2004. Monzonitic series from the Variscan Tormes Dome
796 (Central Iberian Zone): petrogenetic evolution from monzogabbro to granite magmas.
797 Lithos 72, 19-44.
798 McBirney, A.R., Noyes, R.M., 1979. Crystallization and layering of the Skaergaard intrusion.
799 Journal of Petrology 20, 487-554.
800 McEllen, A.T., 2006. Pegmatites of the Mount Sheridan gabbro, Wichita Mountains,
801 Oklahoma. Geological Society of America Abstracts with Programs 38 (1), 5.
802 Momme, P., Wilson, J.R., 2002. The Kraemer Island macrodyke, East Greenland:
803 solidification of a flood basalt conduit. Geological Magazine 139, 171-190.
804 Paterson, S.R., 2009. Magmatic tubes, pipes, troughs, diapirs, and plumes: Late-stage
805 convective instabilities resulting in compositional diversity and permeable networks in
806 crystal-rich magmas of the Tuolumne batholith, Sierra Nevada, California. Geophere 5,
807 496-527.
808 Petford, N., 2009. Which effective viscosity? Mineralogical Magazine 73, 167-191.
809 Peucat, J.J., Ménot, R.-P., Monnier, O., Fanning, C.M., 1999. The Terre Adélie basement in
810 the East-Antarctica shield: geological and isotopic evidence for a major 1.7 Ga thermal

event; comparison with the Gawler Craton in South Australia. Precambrian Research 94, 205-224.

Philpotts, A.R., Carroll, M., Hill, J.M., 1996. Crystal-mush compaction and the origin of pegmatitic segregation sheets in a thick flood-basalt flow in the Mesozoic Hartford Basin, Connecticut. Journal of Petrology 37, 811-836.

Pons, J., Barbey, P., Nachit, H., Burg, J.-P., 2006. Development of igneous layering during growth of pluton: The Tarçouate Laccolith (Morocco). Tectonophysics 413, 271-286.

Roach, R.A., 1971. The layered structure of the St Peter Port Gabbro, Guernsey, Channel Isles (abstract). Journal of the Geological Society of London 127, 295.

Samson, S.D., D'Lemos, R.S., 1998. U-Pb geochronology and Sm-Nd isotopic composition of Proterozoic gneisses, Channel Islands, UK. Journal of the Geological Society of London 155, 609-618.

Samson, S.D., D'Lemos, R.S., 1999. A precise late Neoproterozoic U-Pb zircon age for the syntectonic Perelle quartz diorite, Guernsey, Channel Islands, UK. Journal of the Geological Society of London 156, 47-54.

Schmidt, M.W., 1992. Amphibole composition in tonalite as a fonction of pressure: an experimental calibration of the Al-in-hornblende barometer. Contributions to Mineralogy and Petrology 110, 304-310.

Sparks, R.S.J., Huppert, H.E., 1984. Density changes during fractional crystallization of basaltic magmas: fluid dynamic implications. Contributions to Mineralogy and Petrology 85, 300-309.

Sparks, R.S.J., Huppert, H.E., Koyaguchi, T., Halloworth, M.A., 1993. Origin of modal and rhythmic igneous layering by sedimentation in a convecting magma chamber. Nature 361, 246-249.

835 Sparks, R.S.J., Marshall, L.A., 1986. Thermal and mechanical constraints on mixing between
836 mafic and silicic magmas. Journal of Volcanology and Geothermal Research 29, 99-124.
837 Sparks, R.S.J., Meyer, P., Sigurdsson, H., 1980. Density variation amongst Mid-Ocean Ridge
838 Basalts: implication for magma mixing and the scarcity of primitive lavas. Earth and
839 Planetary Science Letters 46, 419-430.
840 Stewart, B.W., De Paolo, D.J., 1992. Diffusive isotopic contamination of mafic magma by
841 coexisting silicic liquid in the Muskox intrusion. Science 255, 708-711.
842 Sun, S.S., McDonough, W.F., 1989. Chemical and isotopic systematics of oceanic basalts:
843 implication for mantle composition and processes. In: Saunder, A.D., Norry, M.J. (Eds),
844 Geological Society Special Publication. Magmatism in the Ocean Basins, vol. 42.
845 Blackwell, London, p. 313-345.
846 Topley, C.G., Brown, M., D'Lemos, R.S., Power, G.M., Roach, R.A., 1990. The northern
847 igneous complex of Guernsey, Channel Islands. R.S. D'Lemos, R.A. Strachan and C.G.
848 Topley (Editors), The Cadomian Orogeny. Geological Society Special Publication 51,
849 245-259.
850 Topley, C.G., Brown, M., Power, G.M., 1982. Interpretation of field relationships of diorites
851 and associated rocks with particular reference to northwest Guernsey, Channel Islands.
852 Geological Journal 17, 323-343.
853 Waight, T.E., Wiebe, R.A., Krogstad, E.J., 2007. Isotopic evidence for multiple contributions
854 to felsic magma chambers: Gouldsboro Granite, Coastal Maine. Lithos 93, 234-247.
855 Wiebe, R.A., 1974. Coexisting intermediate and basic magmas, Ingonish, Cape Breton Island.
856 Journal of Geology 82, 74-87.
857 Wiebe, R.A., 1993a. Basaltic injections into floored silicic magma chambers. Eos,
858 Transactions, American Geophysical Union 74, 1, 3.

859 Wiebe, R.A., 1993b. The Pleasant Bay layered gabbro-diorite, Coastal Maine: Ponding and
860 crystallization of basaltic injections into a silicic magma chamber. Journal of Petrology
861 34, 461-489.
862 Wiebe, R.A., 1994. Silicic magma chambers as traps for basaltic magmas: The Cadillac
863 Mountain intrusive complex, Mount Desert Island, Maine. Journal of Geology 102, 423-
864 437.
865 Wiebe, R.A., 1996. Mafic-silicic layered intrusions: the role of basaltic injections on
866 magmatic processes and the evolution of silicic magma chambers. Transactions of the
867 Royal Society of Edinburgh: Earth Sciences 87, 233-242.
868 Wiebe, R.A., Collins, W.J., 1998. Depositional features and stratigraphic sections in granitic
869 plutons: implications for the emplacement and crystallization of granitic magma. Journal
870 of Structural Geology 20, 1273-1289.
871 Wiebe, R.A., Frey, H., Hawkins, D.P., 2001. Basaltic pillow mounds in the Vinalhaven
872 intrusion, Maine. Journal of Volcanology and Geothermal Research 107, 171-184.
873 Wiebe, R.A., Smith, D., Sturm, M., King, E.M., Seckler, M.S., 1997. Enclaves in the Cadillac
874 Mountain Granite (Coastal Maine): Samples of hybrid magma from the base of the
875 chamber. Journal of Petrology 38, 393-423.
876 Wiebe, R.A., Wark, D.A., Hawkins, D.P., 2007. Insights from quartz cathodoluminescence
877 zoning into crystallization of the Vinalhaven granite, coastal Maine. Contributions to
878 Mineralogy and Petrology 154, 439-453.
879
880 **Figure captions**
881
882 Fig. 1. Geological sketch maps, location of detailed maps (including those of Fig. 2) and of
883 samples. a. North Armorican domains. b. Saint-Jean-du-Doigt intrusive complex (SJIC), from

884 Chantraine et al. (1986). Ages from Barboni et al. (2010). c. North-Guernsey intrusive
885 complex (NGIC), contours and ages from Bremond d'Ars et al. (1992) and Samson and
886 D'Lemos (1998, 1999).
887
888 Fig. 2. Geological sketch map of noteworthy outcrops and sample location. a. Poul Rodou, b.
889 Roc'h Louet, and c. Primel from the SJIC (this work). d. The Beaucette Battery, and e. The
890 Beaucette pass from the NGIC (this work and Bremond d'Ars et al., 1992).
891
892 Fig. 3. Photographs of sheets and diapirs in the SJIC sampled sections. a. Section SJ34 and
893 sample position. Hammer for scale. b. Section SJ43 and sample position. Hammer for scale.
894 c. A dioritic sheet with feeding roots, under a xenolith. d. A concave-down diapir within the
895 gabbro, just below a not visible dioritic sheet.
896
897 Fig. 4. Mixing, mingling, magmatic brecciation and pegmatoid in the SJIC (Saint-Jean's bay).
898 a. Gabbroic pillow-like enclave with a chilled margin, enclosed in a heterogeneous
899 monzogabbro (mingling). b. Ribbon rocks in the process of hybridization (mingling/mixing).
900 Hammer for scale. c. Jigsaw-type breccias with polyhedral mafic enclaves enclosed in a
901 texturally homogeneous (intergranular) monzonite forming a vein network. A few blocky
902 clasts present mixing/mingling evidence (not visible). d. Mafic cumulate-aplite-pegmatoid
903 association. Sample PM2 (three analyses in Table 1).
904
905 Fig. 5. Sheets and diapirs in the NGIC. a. Photograph of section GS10 and sample position.
906 Hammer for scale. b. Detail: gabbroic sheet and inclined pipes. Pencil for scale. c.
907 Photograph of section GS13 and sample position. d. Sketch of the dioritic veins. e. Sketch of
908 the inclined pipes. f. Cross-section through a zoned pipe, with a core (dark gray) less

909 differentiated than the rim (light gray), a pegmatitic upper part (white), and altered overlying
910 host rock. d, e and f from Elwell et al. (1960).
911
912 Fig. 6. Cumulates and pegmatoids from the NGIC (Spur Point, Saint Peter Port gabbro). a.
913 Mottled orthocumulate showing layers of poikilitic amphibole crystal flecks. Pencil for scale.
914 b. Photomicrograph (crossed nicols) of the Spur Point mottled orthocumulate (sample GS1a,
915 fleck-free white layer). Cumulus minerals are calcic plagioclase (Pl), hornblende (Hb) and
916 clinopyroxene (Cpx). By decreasing abundance, intercumulus phases are plagioclase,
917 clinopyroxene, orthopyroxene, Fe-Ti oxides, and apatite. c. Mafic cumulate-pegmatoid
918 association.
919
920 Fig. 7. NGIC plagioclase compositions. a. Anorthite content in plagioclases of samples GS1a
921 (26 analyses), GS7d, e, l (21 analyses), and GS13a (16 analyses). b. Anorthite profile through
922 a plagioclase from GS13a.
923
924 Fig. 8. Chemical sections in the SJIC. MgO, TiO_2 and Al_2O_3 concentrations through sections
925 SJ34 and SJ43 (located in Fig. 2a and shown in Fig. 3a and b). Microtextural sketches, shown
926 for samples SJ34a, d2, and e, evidence the lack of chilled margins (white: plagioclase; grey:
927 amphibole and altered olivine; black: Fe-Ti oxides).
928
929 Fig. 9. Chemical sections in the NGIC. MgO, TiO_2 and Al_2O_3 contents through sections
930 GS10-13 and GS7 (located in Fig. 2d and e).
931
932 Fig. 10. Magmatic affinities of the mafic rocks from the SJIC and NGIC. Position of the
933 gabbroic samples in the diagram La/10-Y/15-Nb/8 (Cabanis and Lecolle, 1989).

934

935 Fig. 11. Chondrite C1-normalized rare earth elements (REE) patterns of representative SJIC
936 and NGIC samples. Normalization values from Sun and McDonough (1989). a. Sheet-diapir
937 pairs SJ34 and SJ43, together with the corresponding gabbroic field (SJIC). b. Selected SJIC
938 samples. c. Macrorhythms, sheets and a pipe from the NGIC. d. Granite, sheet and cumulate
939 from the NGIC.

940

941 Fig. 12. Models of replenishment and crystallization. Time proceeds along the "*t*-box" line.
942 a. b. c. Model for Poul Rodou in the SJIC. A gabbroic (θ) reservoir crystallizes from below:
943 crystal settling is negligible so that the resulting gabbro is almost homogeneous. A dioritic
944 magma (δ) with about χ=30% phenocrysts enters the crystallizing gabbro. First buoyant at the
945 base, while rising it crosses levels of neutral buoyancy (assuming negligible crystal
946 resorption) where it spreads to form sheets from which diapirs are then extracted. ρ is density
947 at given temperature (calculated from Bottinga and Weill, 1970) and crystal content (χ for δ;
948 grey scale to the right for θ; see text). Insets are detailed zones of a and b.
949 d. e. f. g. h. i. Model for Beaucette in the NGIC. Mafic recharges (d, g) and crystal settling,
950 first of mafic minerals alone (e), second of mafic crystals and plagioclase (f) account for the
951 layering and the heterogeneities of the gabbros. Then late dioritic recharges (h) and
952 subsequent evolution (i, see text) explain most of the observed features.

953

954 Fig. 13. A comprehensive model for the SJIC reservoir. The straight line locates the observed
955 Poul Rodou/Saint-Jean's bay/Primel coastal cross-section. See text for explanations.

Table 1. Chemical data (wt% oxide, ppm element) on whole rock samples from Saint-Jean-du-Doigt and North-Guernsey.

Location		R. Louet	P. Rodou	Primel	Primel	St-J. W	St-J W	St-J E	P. Rodou	P. Rodou	P. Rodou	P. Rodou	P.Rodou	P. Rodou	P. Rodou
Sample		SJ32	SJ44b	SJ16	SJ14	SJ37	SJ9	SJ17	SJ22	SJ34a	SJ34c	SJ34b1	SJ43a	SJ43c	SJ43d
Texture		Cum.	Gr./Cum	Peg.	Dol.	Gr.	Gr.	Gr.	Gr.	Gr.	Gr.	Gr./Cum.	Gr.	Gr.	Gr./Peg.
Emplacement		Cum.	Intrusion	Intrusion	Dyke	Fl. cl	Fl. cl.	Ang. Cl	Intrusion	Intrusion	Sheet	Diapir	Intrusion	Sheet*	Diapir
Type		Melagab.	Melagab.	Gabbro	Gabbro	Mzgab.	Monz.	Q-Monz.	Granite	Gabbro	Diorite	Diorite	Gabbro	Q-Monz.	Q-Monz.
SiO_2	(wt.%)	44.20	47.10	49.20	50.20	53.25	58.60	71.60	76.75	49.70	60.80	58.80	50.00	72.20	74.00
TiO_2		0.80	0.64	1.92	2.22	2.42	1.37	0.35	0.13	1.81	1.24	0.65	1.79	0.33	0.13
Al_2O_3		14.32	14.22	15.40	14.53	14.80	17.75	15.70	12.05	15.00	15.55	16.90	15.42	14.05	10.62
$Fe_2O_3^t$		12.80	9.40	9.80	9.96	11.58	7.00	0.86	1.62	10.90	5.58	5.80	11.25	1.98	4.32
MnO		0.21	0.15	0.14	0.19	0.20	0.10	0.01	0.02	0.19	0.10	0.09	0.18	0.03	0.03
MgO		13.00	13.90	6.85	6.92	3.69	1.92	0.52	0.10	6.80	2.47	1.18	7.23	0.78	0.19
CaO		10.30	8.50	11.47	12.15	7.20	5.00	2.60	0.24	9.40	8.40	14.60	7.38	2.14	8.70
Na_2O		0.88	1.52	2.85	2.69	3.67	5.55	7.00	3.38	2.86	4.50	0.23	2.48	6.85	0.29
K_2O		0.26	0.85	0.48	0.22	1.46	1.49	0.45	4.70	1.13	0.37	0.23	2.30	0.36	0.24
P_2O_5		0.03	0.14	0.14	0.30	0.72	0.32	0.05	0.02	0.23	0.26	0.19	0.25	0.05	0.02
L.O.I.		3.48	3.41	1.27	0.61	0.64	0.81	0.60	0.56	1.83	1.02	1.60	2.08	0.58	1.02
Total		100.07	99.83	99.52	99.99	99.63	99.91	99.74	99.57	99.85	100.29	100.27	100.36	99.35	99.56
Rb	(ppm)	7.5	27.4	17.3	6.4	42.4	42.5	13.5	185	37.5	9.4	7.9	111	8.6	15.5
Sr		142	253	239	145	218	235	243	23	233	322	695	121	84	445
Ba		50	123	91	19	405	405	116	324	286	90	49	330	35	32
Sc		29.0	29.5	47	45	28.0	8.7	4.0	2.5	40	17	6.5	38	5.2	1.2
V		143	210	405	347	265	145	29	4	290	147	90	281	52	32
Cr		216	955	38	103	35	9	10	3.5	255	25	13	225	11	5
Co		70	57	38	47	25	15	3	2	39	11	5	41	5	2
Ni		213	380	44	55	19	9	7	2	70	17	12	72	7	4
Y		9.6	5.6	23.5	38.0	65	38.8	23.5	54	32.5	47.0	33.0	30.5	21.8	9.3
Nb		2.8	2.5	7.9	14.3	37.5	25.0	17.5	30.0	16.0	30.5	21.5	14.0	15.4	5.2
La		2.5	7.1	6.4	10.8	35.0	29.5	12.8	30.0	11.0	20.5	27.0	11.0	10.0	24.5
Ce		5.3	16.0	14.5	25.0	80	60	25.5	86	25.0	45	56	24.0	16.5	38.0
Nd		3.4	10.0	11.2	17.8	45.0	30.5	12.2	28.5	17.0	26.6	27.0	16.0	8.0	11.0
Sm		1.35	2.70	2.95	5.1	10.4	6.4	2.70	6.6	4.7	6.4	5.5	4.5	2.25	1.75
Eu		0.61	0.84	1.10	1.78	2.67	2.62	0.88	0.60	1.56	1.68	1.89	1.44	1.08	1.11
Gd		1.2	2.7	4.1	6.5	11.0	7.2	3.1	6.9	5.7	7.6	5.8	5.2	2.9	2.1
Dy		1.55	2.45	4.1	6.5	10.9	6.4	3.60	8.2	5.5	7.8	5.4	5.4	3.15	1.4
Er		0.9	1.5	2.2	3.7	6.1	3.7	2.3	5.5	3.1	4.6	3.3	3.1	2.2	1.0
Yb		0.90	1.48	2.10	3.42	5.60	3.62	2.38	6.52	2.92	4.46	3.36	2.90	2.20	1.01
Th		0.30	1.15	1.25	0.55	3.50	5.05	14.7	17.3	1.40	6.15	12.3	1.20	13.7	4.50

ICP-AES analyses (analyst: Jo Cotten, Brest). Cum.: Cumulat; Gr.: Granular (broad sense); Peg.: pegmatitic; Dol.: Doleritic; Apl.: Aplitic; Fl. cl.: Fluidal clast; Ang. cl.: Angular clast; Sheet*: upper part of a sheet; L.O.I.: Loss on ignition.

Table 1 (continuation).

Location		Primel	Primel	Primel	Spur	Cobo	Beaucette	Beaucette	Beaucette	Beaucette	Beaucette	Beaucette	Beaucette	Beaucette
Sample		PM2a	PM2b	PM2c	GS1a	GS8	GS10d	GS10f	GS13a	GS10c	GS7a	GS7e	GS7j	GS7c
Texture		Peg.	Apl.	Cum.	Cum.	Gr.	Gr./Cum.	Gr./Cum.	Gr.	Gr.	Gr./Cum.	Gr. /Cum.	Gr./Cum.	Gr.
Emplacement		Intrusion	Intrusion	Cum.	Cum.	Intrusion	Macrorh.	Macrorh.	Sheet	Diapir	Macrorh	Macrorh	Macrorh	Sheet
Type		Gabbro	Gabbro	Gabbro	Gabbro	Granite	Melagab.	Gabbro	Gabbro	Mzdior.	Melagab.	Gabbro	Gabbro	Diorite
SiO_2	(wt.%)	52.60	48.40	49.00	45.30	76.00	47.70	49.70	48.50	61.80	49.30	53.50	51.90	66.20
TiO_2		0.59	0.57	0.39	1.16	0.10	0.57	0.82	1.09	0.06	0.63	0.82	0.74	0.13
Al_2O_3		17.30	17.25	19.20	20.45	12.40	11.75	18.15	20.80	21.40	13.50	16.85	15.80	16.30
$Fe_2O_3^t$		5.16	7.67	5.70	9.55	1.48	10.45	8.93	9.75	1.35	9.00	8.60	8.15	1.60
MnO		0.09	0.11	0.09	0.13	0.05	0.17	0.15	0.14	0.03	0.14	0.14	0.12	0.02
MgO		6.50	8.85	7.34	5.56	0.24	14.35	6.09	3.60	1.14	12.30	5.23	7.35	1.08
CaO		12.45	12.15	14.10	14.00	0.55	9.20	10.40	9.75	5.32	9.60	8.18	9.40	7.10
Na_2O		3.40	2.21	2.17	1.75	3.61	1.20	2.88	3.40	5.89	2.08	3.21	3.00	5.20
K_2O		0.32	0.13	0.13	0.97	3.23	0.88	0.80	1.03	1.51	0.95	1.38	1.25	0.52
P_2O_5		0.10	0.04	0.03	0.21	0.04	0.09	0.14	0.27	0.05	0.08	0.14	0.12	0.17
L.O.I.		1.61	2.27	2.02	1.07	0.92	3.25	1.45	1.59	1.46	2.12	1.73	1.91	1.98
Total		100.12	99.65	100.17	100.15	98.62	99.61	99.51	99.92	100.01	99.70	99.78	99.74	100.30
Rb	(ppm)	11.5	3.3	3.7	27.2	124	26.0	20.0	29.5	42.0	28.0	40	35.0	13.2
Sr		277	217	266	872	113	172	420	590	867	340	430	340	280
Ba		54	25	22	300	656	298	226	481	351	370	310	190	88
Sc		44	44	44	38	3.3	37	34	26.0	3.9	40	31	44	5
V		184	202	154	317	8	205	253	246	12	210	242	232	28
Cr		179	232	240	72	4	855	195	18	8	1100	138	370	6
Co		25	35	25	32	2	59	31	24	5	50	30	37	7
Ni		50	72	70	24	2	242	42	9	12	265	35	86	8
Y		16.8	14.6	8.8	16.0	12.2	12.6	17.3	24.8	4.4	16.0	19	16.0	6.5
Nb		2.7	1.2	0.4	5.2	11.2	2.3	3.2	6.0	0.7	2.5	4.2	3.7	1.0
La		3.4	2.6	1.7	11.2	18.0	7.8	11.2	15.6	10.5	8.0	12.5	9.4	12.5
Ce		9.5	6.0	4.0	27.0	34.5	15.5	23.5	35	15	18.0	26.0	21.0	22.0
Nd		6.1	4.3	2.0	18.0	12.8	8.4	12.7	22.0	4.2	10.0	14.1	12.1	8.0
Sm		2.00	1.80	1.10	4.2	2.35	2.05	3.0	4.8	0.6	2.75	3.4	3.1	1.5
Eu		0.83	0.90	0.55	1.45	0.43	0.75	1.09	1.40	0.64	0.88	0.99	0.94	0.59
Gd		2.8	2.5	1.55	3.5	2.5	1.9	3.0	4.5	0.6	2.6	3.65	2.8	1.6
Dy		2.85	2.55	1.55	2.95	2.10	2.05	2.90	4.3	0.65	2.65	3.15	2.80	1.15
Er		1.6	1.5	0.8	1.5	1.3	1.3	1.7	2.4	0.5	1.6	1.9	1.6	0.6
Yb		1.50	1.31	0.78	1.30	1.49	1.18	1.67	2.28	0.56	1.62	1.83	1.58	0.57
Th		0.15	0.20	0.10	0.20	11.4	1.35	1.35	1.45	2.75	2.85	3.5	1.90	3.40

Table 2. Isotopic data on whole rock samples from Saint-Jean-du-Doigt and North-Guernsey.

Location	Type	Sample	Rb ppm	Sr ppm	$^{87}Rb/^{86}Sr$	$^{87}Sr/^{86}Sr$	$\pm 2\sigma m$ ($x10^{-6}$)	$(^{87}Sr/^{86}Sr)_i$	Sm ppm	Nd ppm	$^{147}Sm/^{144}Nd$	$^{143}Nd/^{144}Nd$	$\pm 2\ \sigma m$ ($x10^{-6}$)	ε_{Nd}
Saint-Jean-du-Doigt								*(t = 347 Ma)*						*(t = 347 Ma)*
Primel	Dolerite	SJ14	5.98	142	0.122	0.704655	11	0.7041	4.88	17.51	0.1684	0.512846	6	5.3
Primel	Peg.	SJ16	18.5	243	0.221	0.704947	9	0.7039	3.02	10.43	0.1750	0.512829	6	4.7
P. Rodou	Gabbro	SJ34a	38.0	230	0.477	0.707216	9	0.7049	4.22	15.88	0.1609	0.512860	4	5.9
P. Rodou	Diorite	SJ34c	8.71	296	0.085	0.707338	10	0.7069	6.28	25.38	0.1496	0.512668	7	2.6
St-J. W	Mzgab.	SJ37	42.1	208	0.586	0.707246	12	0.7043	10.04	43.62	0.1391	0.512633	7	2.4
St-J. W	Monz.	SJ9	42.3	226	0.541	0.707339	30	0.7047	6.36	30.04	0.1279	0.512632	5	2.9
St-J. E	Q-Monz.	SJ17	14.0	241	0.167	0.707263	10	0.7064	2.55	10.95	0.1407	0.512676	6	3.2
P. Rodou	Granite	SJ22	185	21.6	25.1	0.819524	15	0.6935	5.86	26.58	0.1334	0.512650	5	3.0
North-Guernsey (data from Brémond d'Ars et al., 1992)								*(t = 553 Ma)*						
Spur	Cum.	64A (GS1a)	18.1	891	0.059	0.70627	-	0.7058						
Beaucette	Melag.	27A (GS7a)	34.2	275	0.360	0.70842	-	0.7056						
Beaucette	Gabbro	26B (GS10f)	41.9	379	0.321	0.70836	-	0.7058						
Beaucette	G. sheet	27E (GS13a)	73.7	564	0.378	0.70867	-	0.7057						
Cobo	Granite	74-71 (GS8)	127	101	3.64	0.73417	-	0.7055						

See text for analytical methods and calculation of ε_{Nd}; index i for initial.

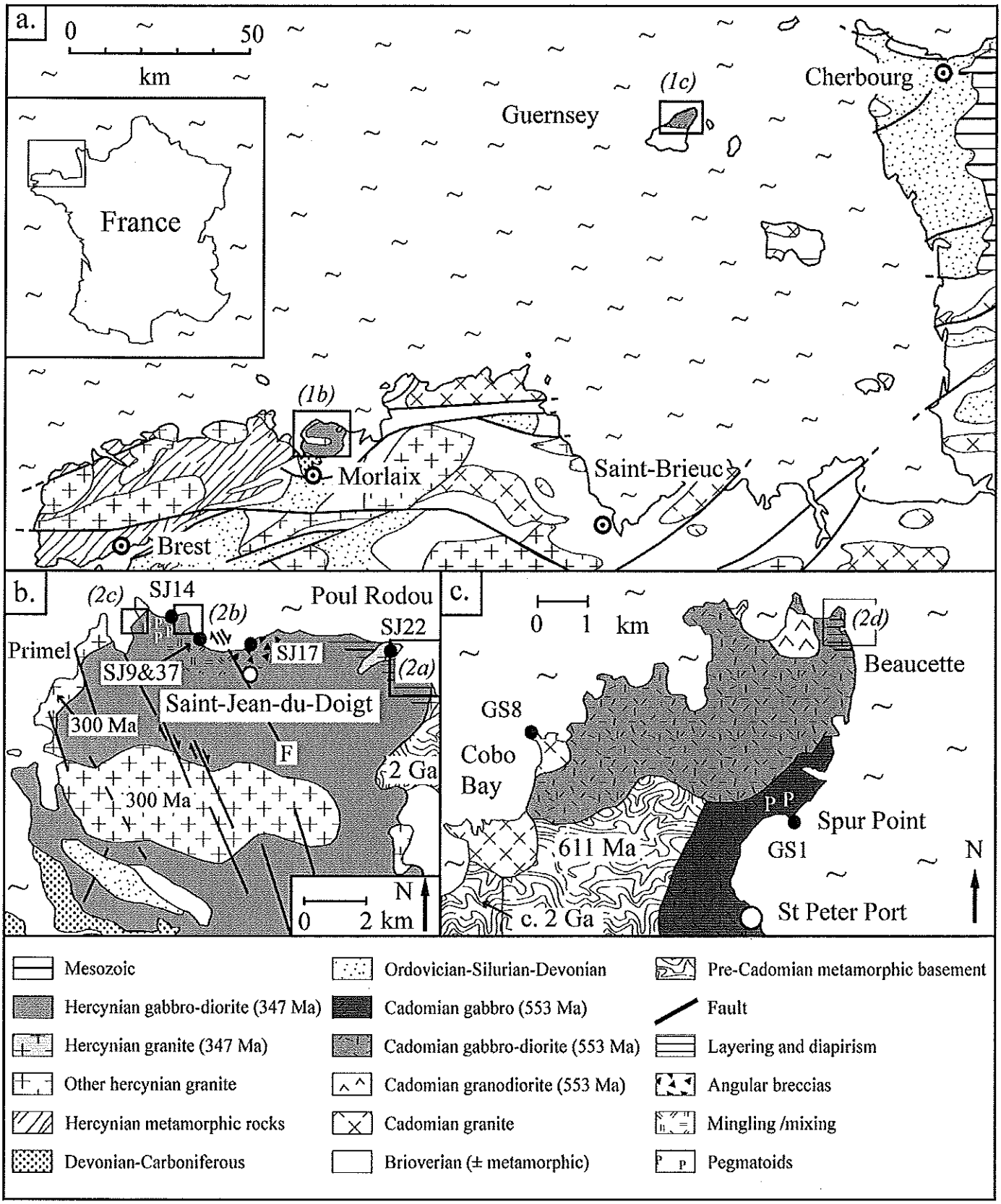
a.
0
50
km
France
Guernsey
(1c)
Cherbourg
(1b)
Morlaix
Saint-Brieuc
Brest
b.
(2c)
SJ14
(2b)
Poul Rodou
SJ22
Primel
SJ9&37
SJ17
(2a)
Saint-Jean-du-Doigt
300 Ma
F
2 Ga
300 Ma
N
0
2 km
c.
0
1
km
(2d)
Beaucette
GS8
Cobo
Bay
Spur Point
GS1
611 Ma
N
St Peter Port
c. 2 Ga
Mesozoic
Hercynian gabbro-diorite (347 Ma)
Hercynian granite (347 Ma)
Other hercynian granite
Hercynian metamorphic rocks
Devonian-Carboniferous
Ordovician-Silurian-Devonian
Cadomian gabbro (553 Ma)
Cadomian gabbro-diorite (553 Ma)
Cadomian granodiorite (553 Ma)
Cadomian granite
Brioverian (± metamorphic)
Pre-Cadomian metamorphic basement
Fault
Layering and diapirism
Angular breccias
Mingling /mixing
Pegmatoids

Fig. 1

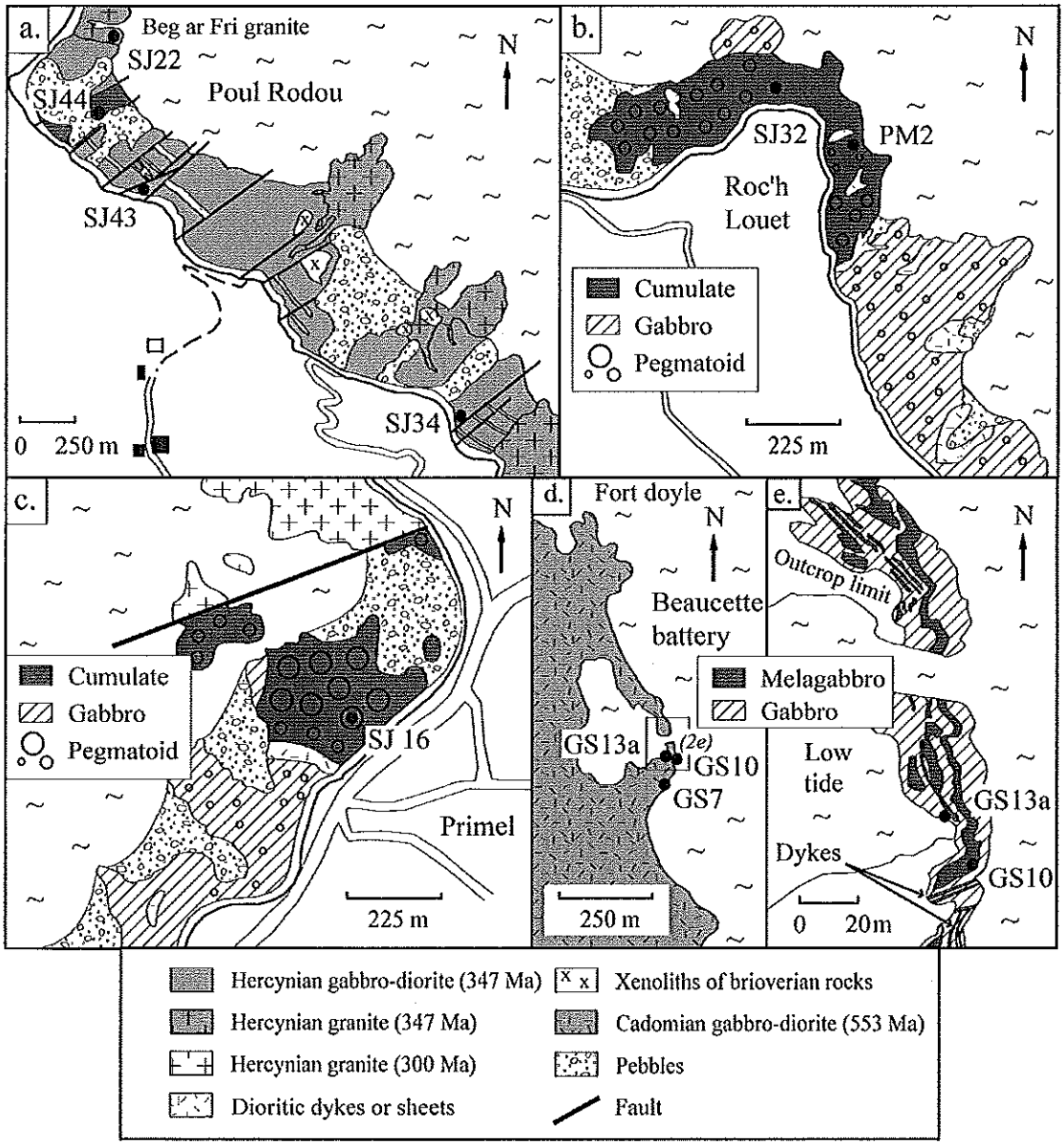
a.
Beg ar Fri granite
SJ22
SJ44
Poul Rodou
SJ43
SJ34
N
0 250 m
b.
SJ32
PM2
Roc'h
Louet
Cumulate
Gabbro
Pegmatoid
225 m
c.
Cumulate
Gabbro
Pegmatoid
SJ 16
Primel
225 m
d.
Fort doyle
Beaucette
battery
GS13a
(2e)
GS10
GS7
250 m
e.
Outcrop limit
Melagabbro
Gabbro
Low
tide
GS13a
Dykes
GS10
0 20m
Hercynian gabbro-diorite (347 Ma)
Hercynian granite (347 Ma)
Hercynian granite (300 Ma)
Dioritic dykes or sheets
Xenoliths of brioverian rocks
Cadomian gabbro-diorite (553 Ma)
Pebbles
Fault

Fig. 2

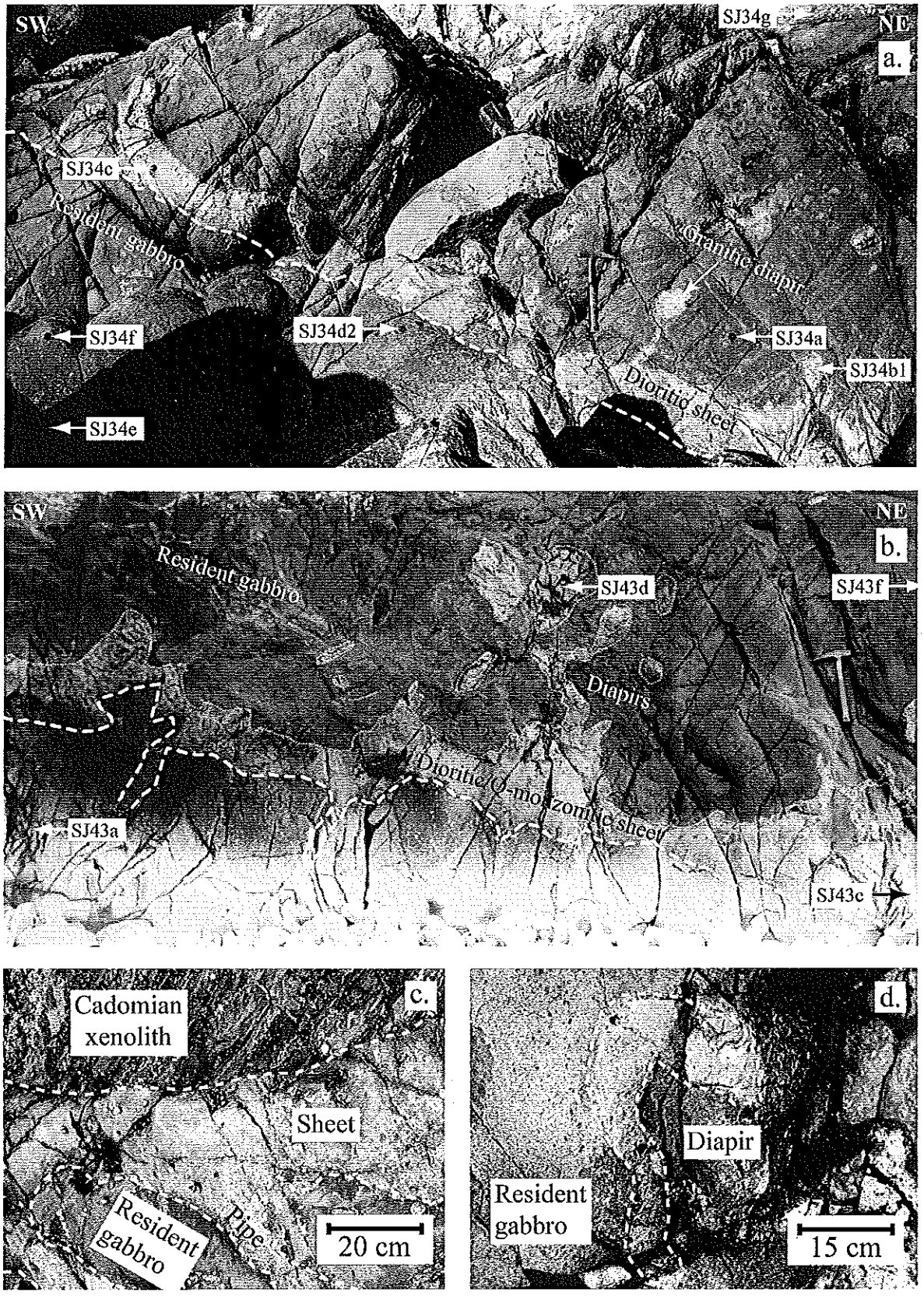
SW
SJ34g
NE
a.
SJ34c
Resident gabbro
Granitic diapir
SJ34f
SJ34d2
SJ34a
SJ34b1
Dioritic sheet
SJ34e
SW
NE
b.
Resident gabbro
SJ43d
SJ43f
Diapirs
Diorite/Q-monzonite sheet
SJ43a
SJ43c
Cadomian xenolith
c.
Sheet
Resident gabbro
Pipe
20 cm
d.
Diapir
Resident gabbro
15 cm

Fig. 3

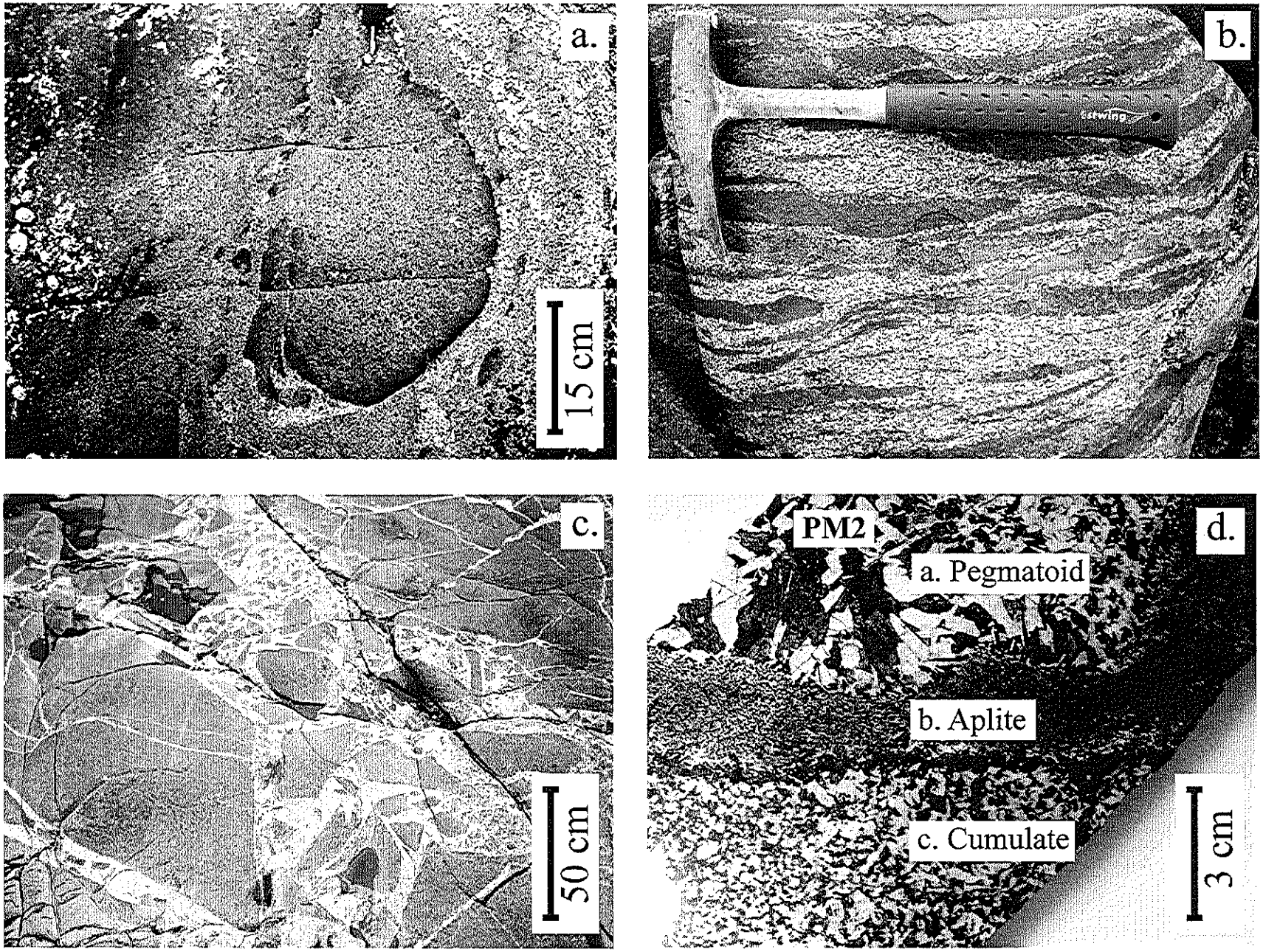

Fig. 4

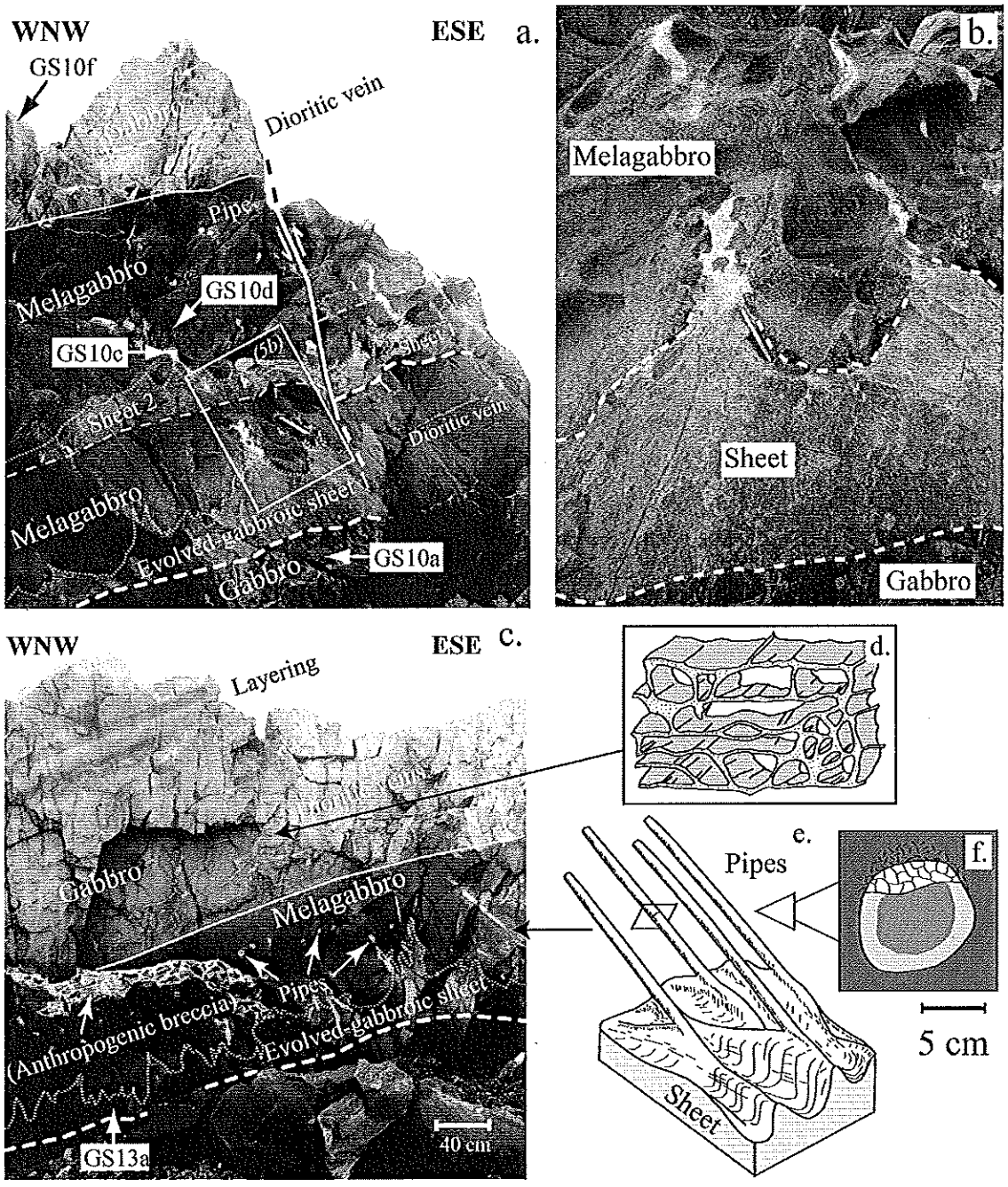
WNW
ESE
a.
GS10f
Dioritic vein
Pipes
Melagabbro
GS10d
GS10c
(5b)
Sheet 1
Sheet 2
Dioritic vein
Melagabbro
Evolved gabbroic sheet
Gabbro
GS10a
b.
Melagabbro
Sheet
Gabbro
WNW
ESE
c.
Layering
Gabbro
Melagabbro
Pipes
(Anthropogenic breccia)
Evolved gabbroic sheet
GS13a
40 cm
d.
e.
Pipes
f.
5 cm
Sheet

Fig. 5

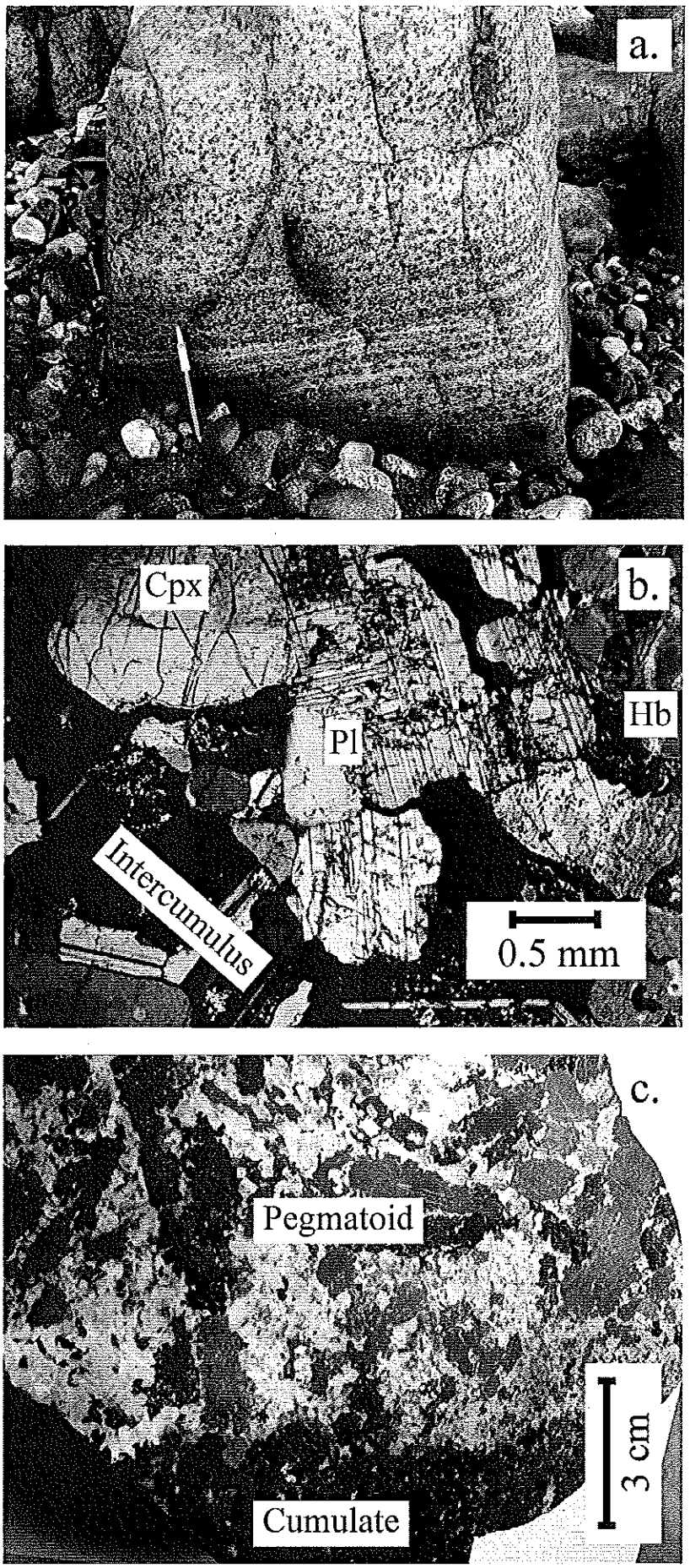

Fig. 6

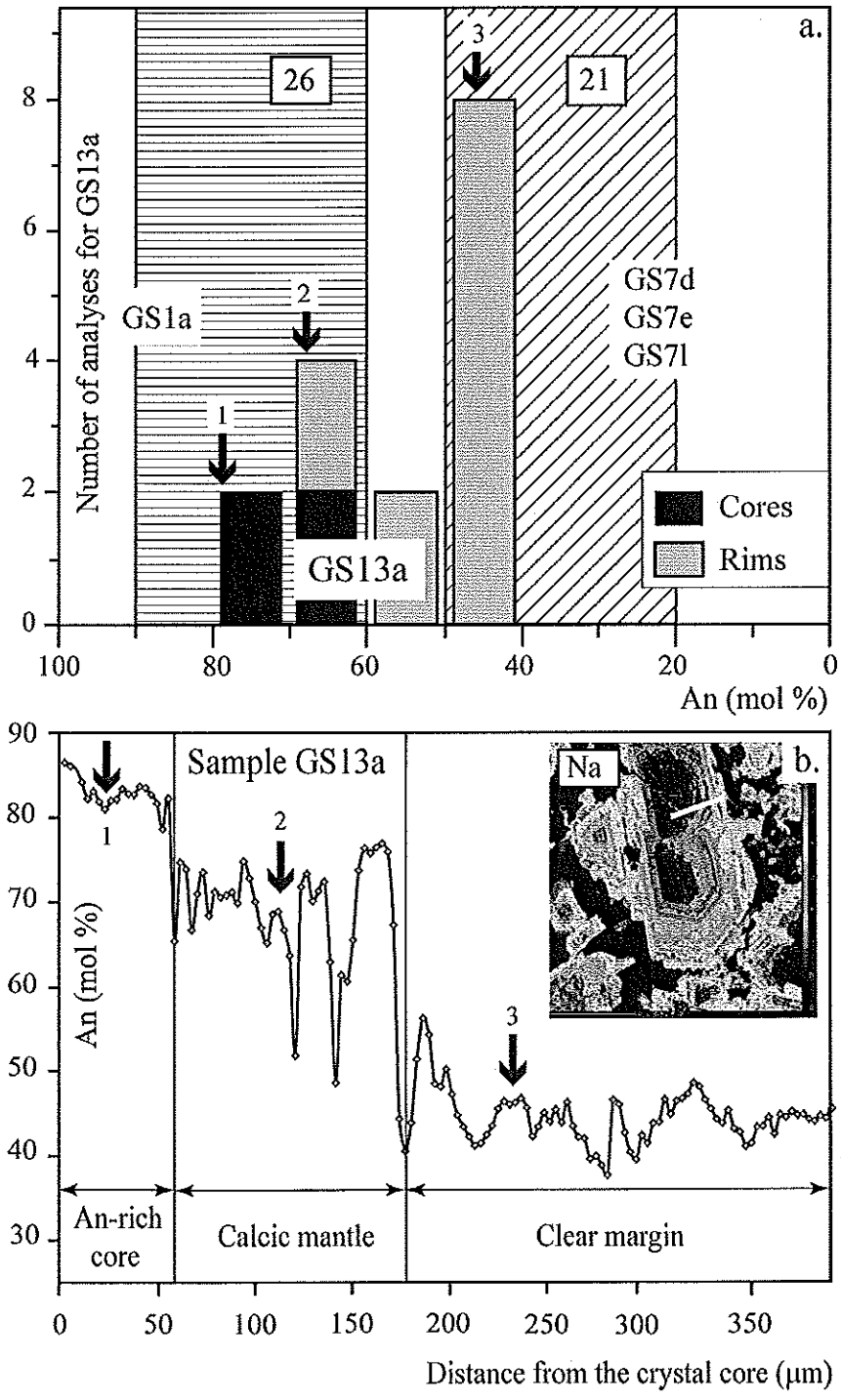
a.
26
21
3
2
1
GS1a
GS13a
GS7d
GS7e
GS7l
Cores
Rims
Number of analyses for GS13a
An (mol %)
b.
Sample GS13a
Na
An (mol %)
An-rich core
Calcic mantle
Clear margin
Distance from the crystal core (μm)

Fig. 7

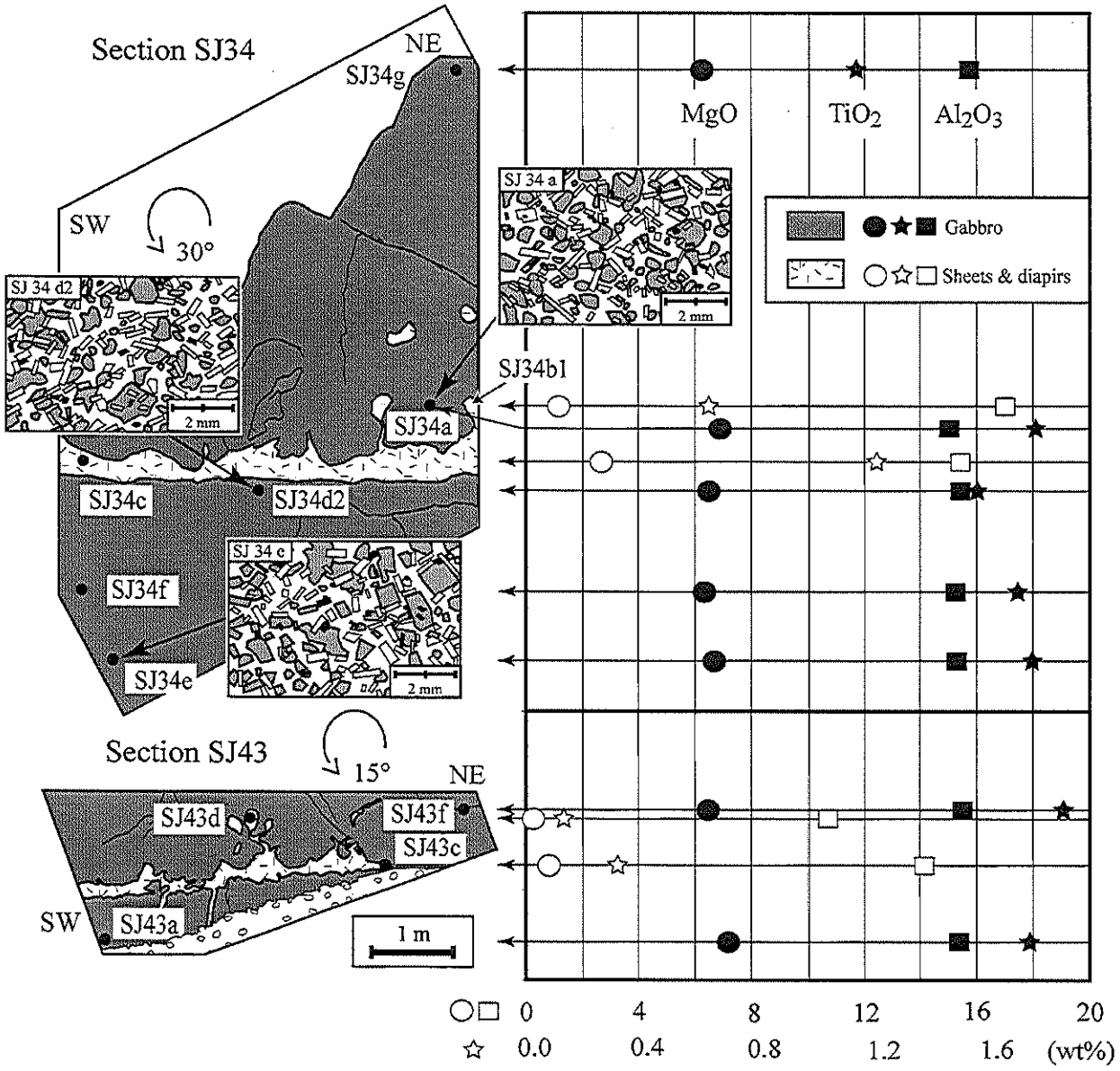
Section SJ34
NE
SJ34g
SW
30°
SJ 34 d2
2 mm
SJ34a
SJ34c
SJ34d2
SJ 34 c
SJ34f
SJ34e
2 mm
Section SJ43
15°
NE
SJ43d
SJ43f
SJ43c
SW
SJ43a
1 m
SJ 34 a
2 mm
SJ34b1
MgO
TiO2
Al2O3
Gabbro
Sheets & diapirs
0
4
8
12
16
20
0.0
0.4
0.8
1.2
1.6
(wt%)

Fig. 8

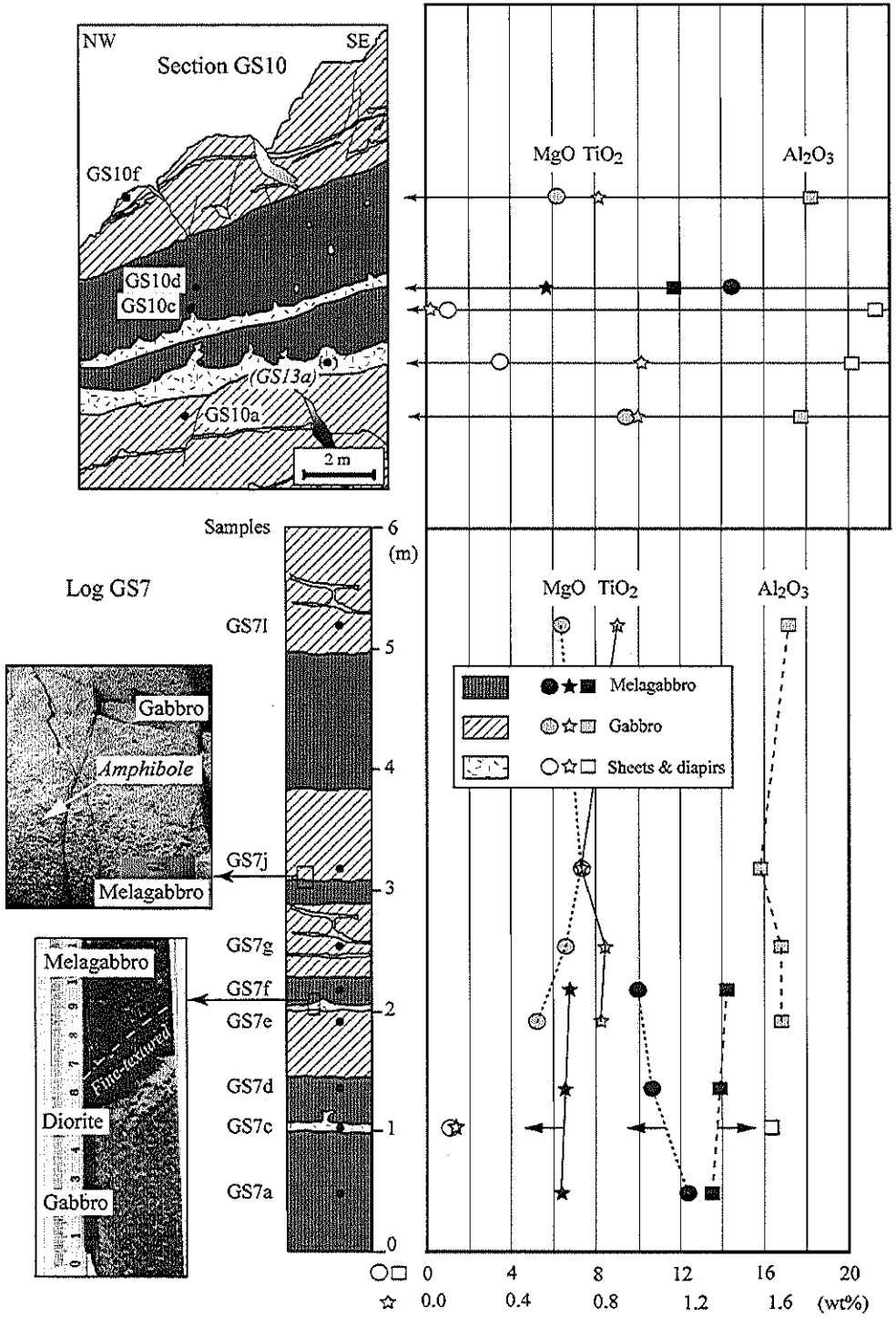
NW
SE
Section GS10
GS10f
GS10d
GS10c
(GS13a)
GS10a
2 m
Samples
Log GS7
GS7l
GS7j
GS7g
GS7f
GS7e
GS7d
GS7c
GS7a
Gabbro
Amphibole
Melagabbro
Melagabbro
Fine-textured
Diorite
Gabbro
6
(m)
5
4
3
2
1
0
MgO TiO2
Al2O3
MgO TiO2
Al2O3
Melagabbro
Gabbro
Sheets & diapirs
0
4
8
12
16
20
0.0
0.4
0.8
1.2
1.6
(wt%)

Fig. 9

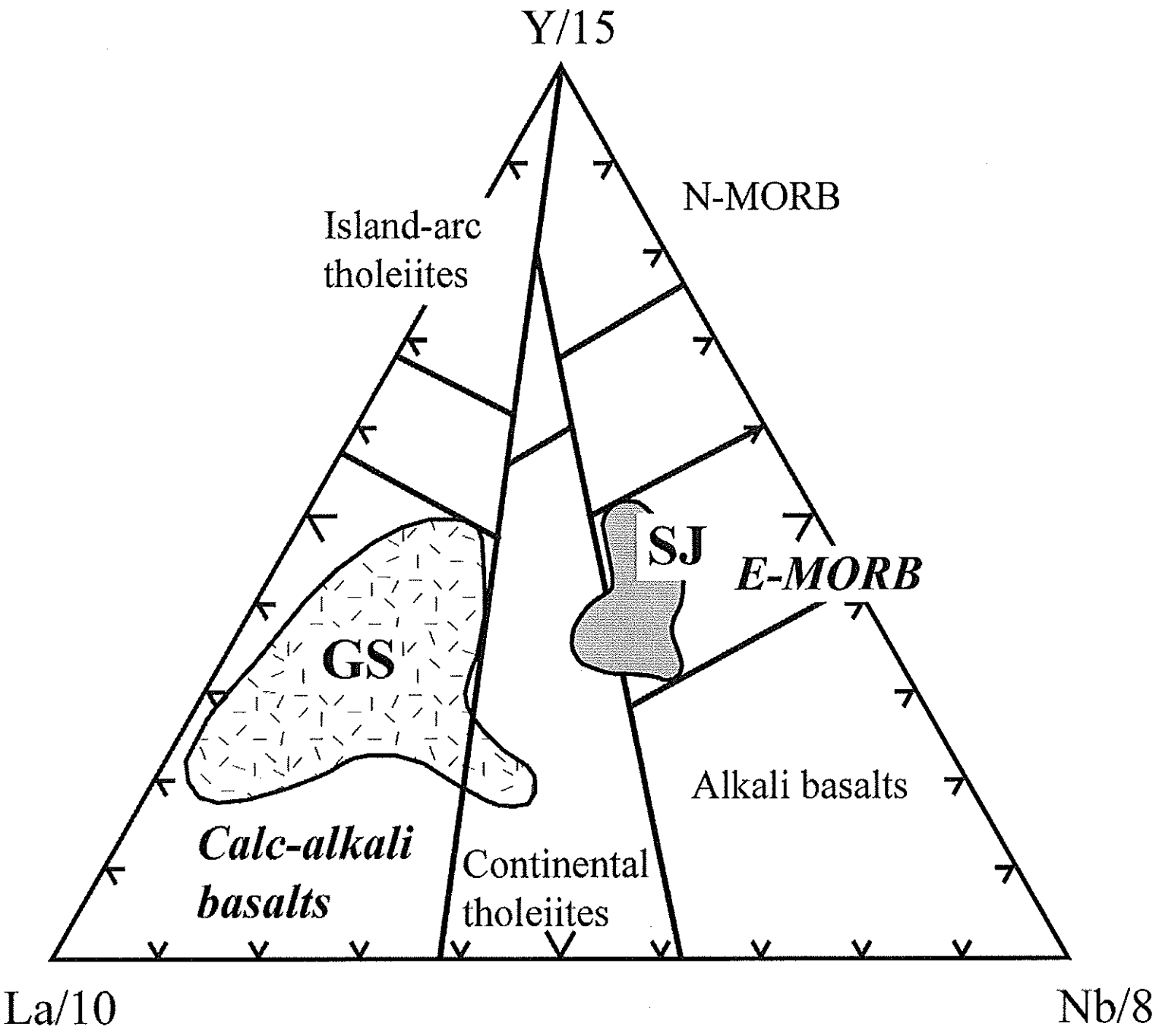
Y/15
Island-arc
tholeiites
N-MORB
SJ
E-MORB
GS
Alkali basalts
Calc-alkali
basalts
Continental
tholeiites
La/10
Nb/8

Fig. 10

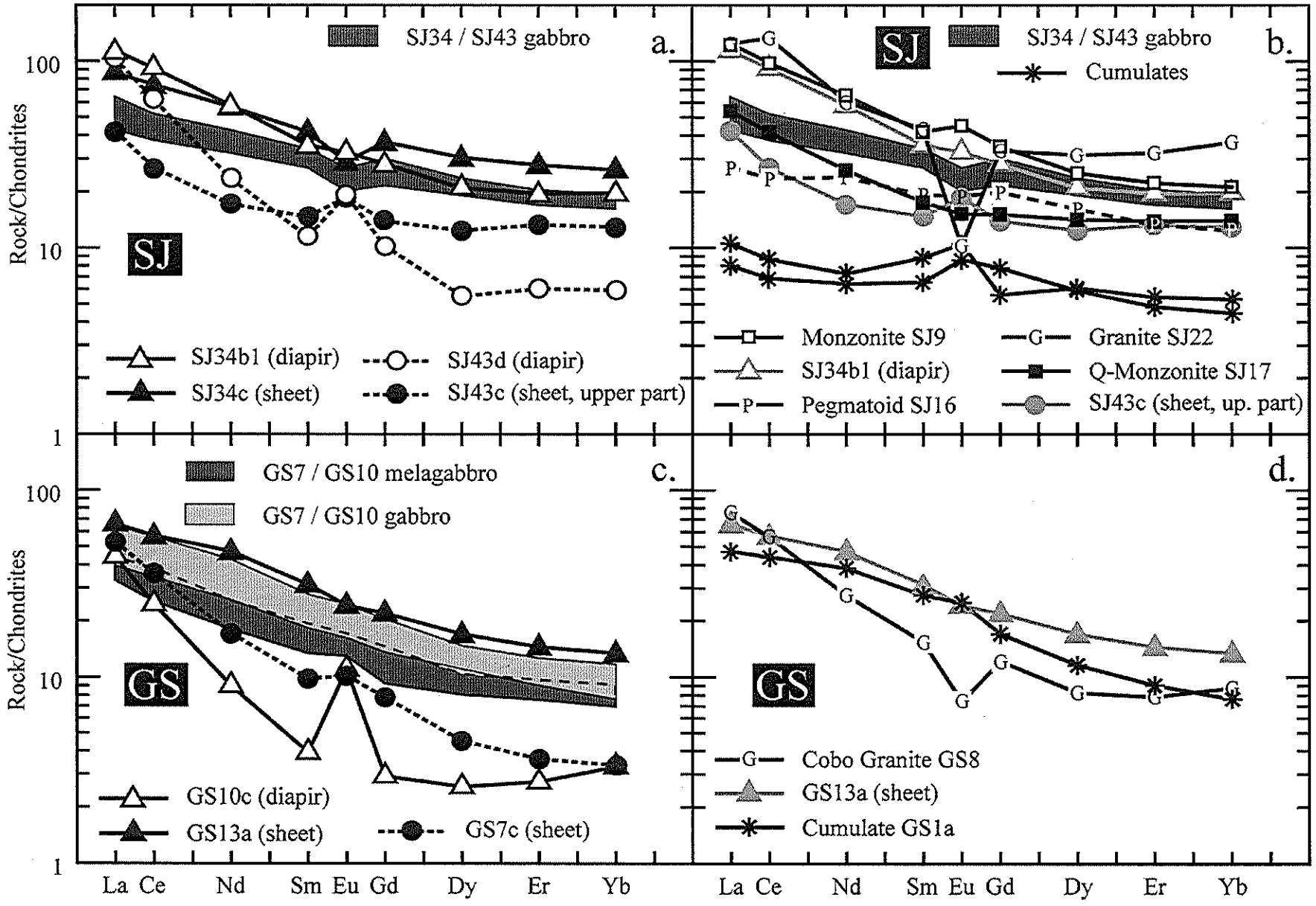
a.
SJ34 / SJ43 gabbro
SJ
SJ34b1 (diapir)
SJ34c (sheet)
SJ43d (diapir)
SJ43c (sheet, upper part)
b.
SJ
SJ34 / SJ43 gabbro
Cumulates
Monzonite SJ9
SJ34b1 (diapir)
Pegmatoid SJ16
Granite SJ22
Q-Monzonite SJ17
SJ43c (sheet, up. part)
c.
GS7 / GS10 melagabbro
GS7 / GS10 gabbro
GS
GS10c (diapir)
GS13a (sheet)
GS7c (sheet)
d.
GS
Cobo Granite GS8
GS13a (sheet)
Cumulate GS1a
Rock/Chondrites
100
10
1
La Ce Nd Sm Eu Gd Dy Er Yb

Fig. 11

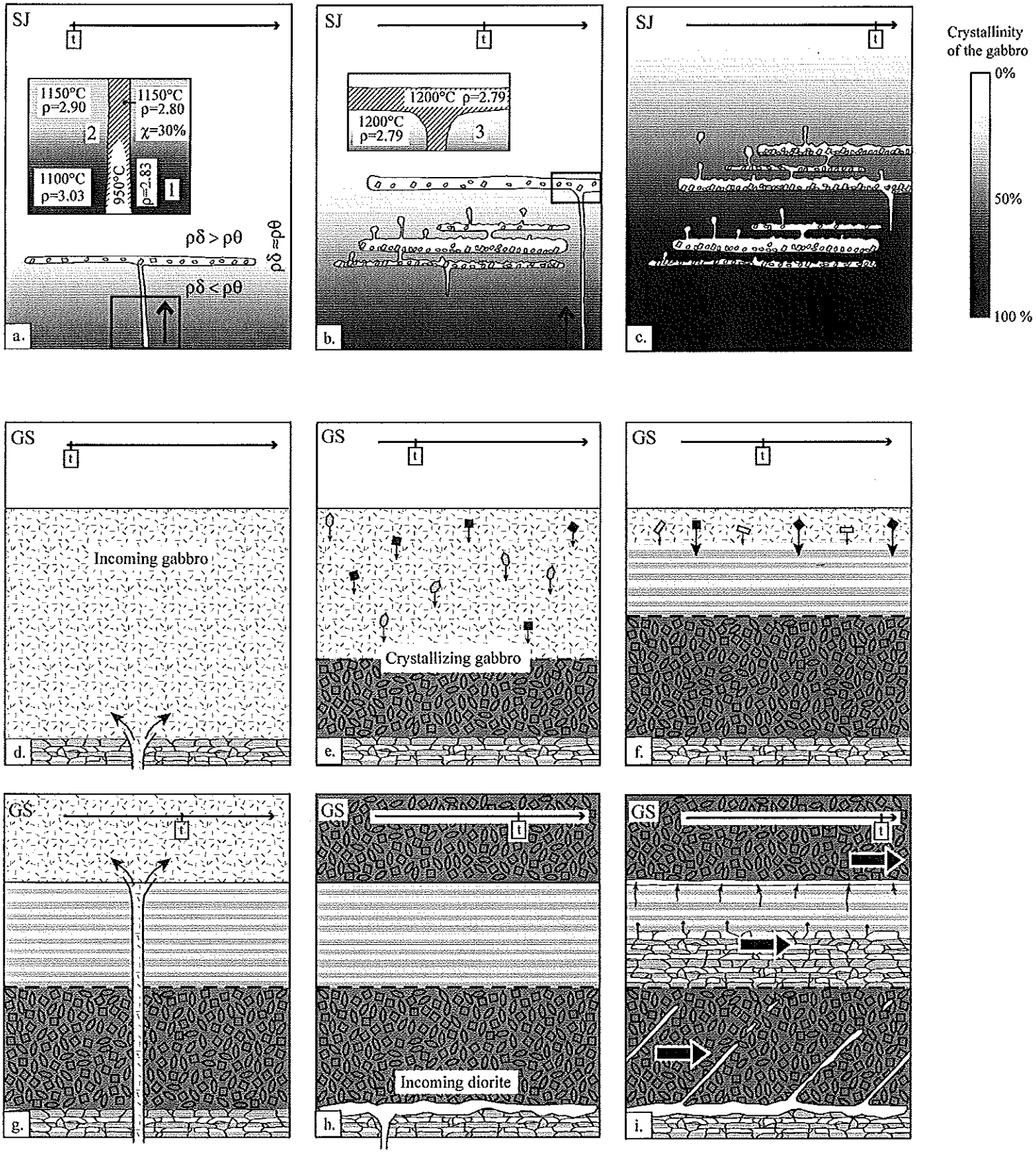
SJ
t
1150°C
ρ=2.90
2
1150°C
ρ=2.80
χ=30%
1100°C
ρ=3.03
950°C
ρ=2.83
1
ρδ > ρθ
ρδ ≈ ρθ
ρδ < ρθ
a.
SJ
t
1200°C ρ=2.79
1200°C
ρ=2.79
3
b.
SJ
t
c.
Crystallinity
of the gabbro
0%
50%
100 %
GS
t
Incoming gabbro
d.
GS
t
Crystallizing gabbro
e.
GS
t
f.
GS
t
g.
GS
t
Incoming diorite
h.
GS
t
i.

Fig. 12

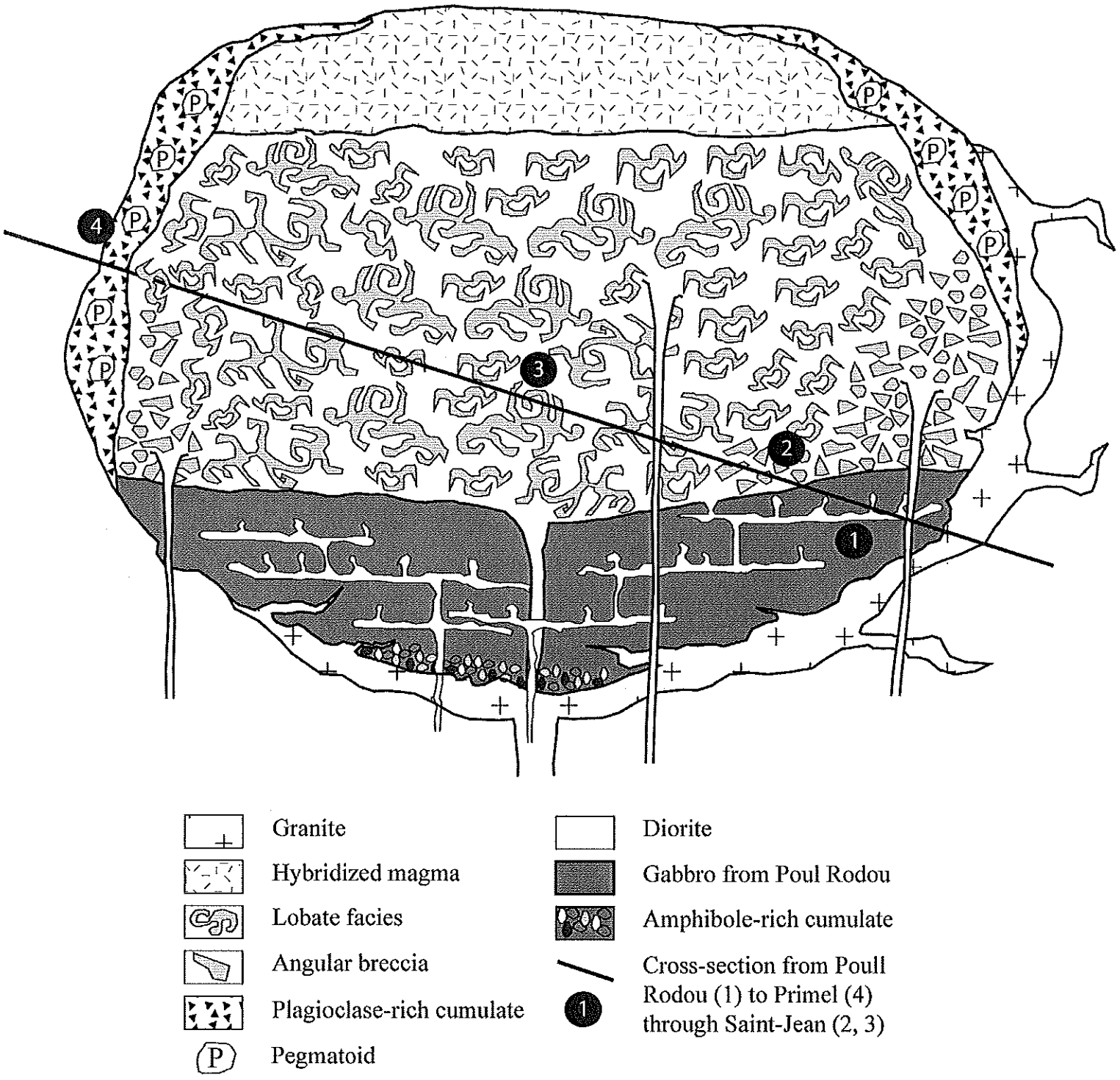
P
4
3
2
1
Granite
Hybridized magma
Lobate facies
Angular breccia
Plagioclase-rich cumulate
Pegmatoid
Diorite
Gabbro from Poul Rodou
Amphibole-rich cumulate
Cross-section from Poull Rodou (1) to Primel (4) through Saint-Jean (2, 3)

Fig. 13